TRIBOLOGICAL CHARACTERIZATION OF COATINGS AND NANOFLUIDS

A Thesis

by

JUHI BAXI

Submitted to the Office of Graduate Studies of
Texas A&M University
in partial fulfillment of the requirements for the degree of

MASTER OF SCIENCE

August 2008

Major Subject: Mechanical Engineering

TRIBOLOGICAL CHARACTERIZATION OF COATINGS AND NANOFLUIDS

A Thesis

by

JUHI BAXI

Submitted to the Office of Graduate Studies of
Texas A&M University
in partial fulfillment of the requirements for the degree of

MASTER OF SCIENCE

Approved by:

Chair of Committee,	Hong Liang
Committee Members,	Richard Griffin
	Melissa Grunlan
Head of Department,	Dennis O'Neal

August 2008

Major Subject: Mechanical Engineering

ABSTRACT

Tribological Characterization of Coatings and Nanofluids.

(August 2008)

Juhi Baxi, B.E., Gujarat University, India

Chair of Advisory Committee: Dr. Hong Liang

Advancement in biotechnology has successfully converted the conventional bearing couples into artificial joints. Materials used today, however, have not been satisfactory. Problems such as osteolysis and aseptic loosening lead to failure of artificial joints and also the lifespan of these joints is to be further improved. This research targets two issues related to the problem: coatings and design of new generation biofluids.

Superior to metals and polymers, ceramics are hard and biocompatible and exhibit low wear and friction. The ceramic-on-ceramic bearing pair could last for a long time which could be beneficial to younger and active patients who need a bearing pair which would last for more than 15 years to avoid the possibility of a revision surgery. The first part of this thesis deals with studying the microstructure-property relationship of new ceramic-based materials and coatings. Specifically, alumina (ceramic) coatings at different current intensities were tested in order to determine their feasibility as a biomaterial for artificial joints.

In order to find a new avenue for developing biofluids, the second part of this thesis focuses on the failure of artificial joints under inadequate lubrication. Also due to osteoarthritis, synthetic biofluid is injected into joints to help relieve pain but it works

for only 6-9 months. We propose a new method using noble gold nanoparticles to modify fluids. This was accomplished by mixing different concentration of nanoparticles with biofluid.

This thesis consists of 6 sections. The first section is an introduction to tribology, biotribology and artificial joints which is followed by the second section which discusses the objectives of the research. The third section describes the materials and methods used in the research. The tribological characterization of MAO alumina coatings is discussed in the fourth section and the fifth section discusses the effect of nanoparticles on fluid lubrication. The last section is the conclusion.

DEDICATION

To my dada,
My beloved parents
&
Aditya

ACKNOWLEDGEMENTS

In any work, that one undertakes, one can not rule out the importance of guidance and assistance, which is as vital as technical information in its completion. I would like to thank my advisor and my mentor Dr Hong Liang for her unconditional support, patience and constant encouragement. Her advice and guidance did not only help me to advance my technical and research skills but will also help me in the future. I would like to extend my gratitude to all my committee members: Dr Richard Griffin and Dr Melissa Grunlan, for their co-operation in my Master's study. I would also like to thank Dr Subrata Kundu for helping me in my research with his expertise in nanoparticles and skills in microscopy and Giridhar Sekar, a biochemist, who taught me about protein structures and that the world of protein is not as simple as it appears. I also appreciate the support and encouragement of the entire Surface Science lab members especially Aracely Rocha, Dedy Ng and Presenjit Kar.

Lastly, my heartfelt gratitude to my parents, Vaishal Acharya, Asit kaka and Neeru kaki, my family and my friends in College Station and back home for their constant love, support and motivation.

TABLE OF CONTENTS

Page

LIST OF FIGURES

FIGURE Page

FIGURE Page

LIST OF TABLES

1. INTRODUCTION TO TRIBOLOGY

This section introduces tribology, history of tribology, friction, wear and lubrication. The main focus of this section is biotribology, artificial prosthesis and lubrication of the Synovial joints.

1.1 Introduction

The word 'Tribology' was first coined by the Working group set up by the Minister of state for education and science in 1966 in England[1]. It is derived from the two Greek words 'tribos' meaning 'rubbing' and 'logos' meaning study[2]. Thus it is the science of rubbing surfaces. Tribology was defined by the British Lubrication Engineering Working group as "the science and technology of interacting surfaces in relative motion and of related subjects and practices"[3]. Tribology combines the study of the three interdisciplinary fields: friction, wear and lubrication. Even though the name is relatively new the importance of the constitutive parts of tribology is very old. It is of significant economic importance[1,4] and is applicable to all fields such as memory device technology, bioengineering, space engineering, nanodevices etc. Tribology applied to biological fields is called Biotribology[5] which will be covered in the later sections and is the main focus of this thesis.

This thesis follows the style of Tribology Letters.

1.2 History of Tribology

It is speculated that the first fires in the Stone Age were started using friction[6]. The earliest known bearings used to drill holes to start the fire were made with bones or antlers[7] and then later replaced with wood, stone, cotton and potter's wheel.

The earliest record of the use of lubricants in order to reduce friction was in the bearings of chariots in 3500 B.C.[8] Water was also used as a lubricant as early as 2400 B.C. In a temple panting of 2000 B.C. a man is shown pouring oil to facilitate the movement of the colossus[9]. Evidence of the use of animal fat as a lubricant has also been discovered in the Egyptian tombs of the 15th century.

The scientific study of friction began when Leonardo da Vinci deduced the rules of friction. But his work remained unpublished[10]. Guillaume Amontons rediscovered the friction laws in 1696[11]; he stated that the friction was dependent on the weight and not on the area of contact. De a Hire, a senior academician proved the independence of friction on the area of contact[12]. He postulated that the solid body has many irregularities and when these interlock then they either abrade or deform during relative motion. Coulomb postulated that the friction existed due to the contact between the asperities of the two mating surfaces[13]. Today the friction law is called Coulomb's law or Amontons law or Coulomb-Amontons law. Jon Leslie proposed that friction was due to the work done by deformation of the roughness on the surface.

The scientific study of lubrication began with Osborne Reynolds who developed the hydrodynamic lubrication theory[14], based on the research of Petrov and Tower. Petrov later discovered that viscosity and not density was the most important factor in

fluid lubrication and that the viscous shearing of the fluid resulted in frictional losses[15,16,17,18]. While Tower established that the clearance between the journal and sleeve dictated the load bearing capability and that it was a vital component in reducing friction and achieving full film lubrication[19,20]. After their initial pioneering work, later subsequent work was carried forward by Stokes[21], Mitchell[22], Sommerfield and many others.

As compared to both friction and lubrication, the study on wear and wear mechanisms is relatively new. The importance of wear and the economic losses that followed has made the study of wear very pertinent. However the quantification of wear and wear rate is fraught with lot of complications, since wear and wear rate depends upon many unpredictable conditions such as: material, geometry of surfaces, surface asperity, surface roughness, elastic properties etc[23]. "Archard's Wear Law" has been the most noteworthy effect in that direction[24].

1.3 Friction, Wear and Lubrication

1.3.1 Friction

Friction reduces the relative motion between the two bodies or resists the tendency to motion between the two bodies in contact. The main reason for wear and energy losses is friction. The friction between the two mating surfaces depends upon the geometry, macroscopic contact points, elastic properties, adhesive forces, deformation of the surface during movement etc[25]. There are basically two types of friction: Internal friction and external friction. External friction is the mechanical force which resists or

hinders movement between two surfaces whereas the internal friction is the friction between lubricant molecules[26].

According to Coulomb-Amontons law, the coefficient of friction is a dimensionless number and is defined as the ratio of the force and the normal load[13]. The different types of friction are[26]:

1. Sliding friction
2. Rolling friction
3. Static friction
4. Kinetic friction
5. Stick-slip

Sliding friction is due to purely sliding motion between the two surfaces[27] e.g. block sliding on a horizontal plane while rolling friction is the friction generated by rolling contact[28] e.g. friction between the circumference of a wheel and the road. The maximum force that must be overcome to initiate any movement between the two bodies is called the static friction whereas kinetic friction comes into play when the two bodies are in relative motion[29]. The friction which prevents a car from slipping when it is parked on a slope is the static friction while the friction between a sledge moving on the ground is kinetic friction. Stick-slip occurs when the static friction is more than the kinetic friction and hence the motion will be intermittent and slow. The two surfaces will stick till the sliding force becomes equal to the static friction and then the surfaces will move and then stick again[30]. e.g. lathes, milling machines etc.

1.3.2 Wear

According to the German DIN standard 50 320, "the progressive loss of material from the surfaces of contacting body as a result of mechanical causes" is defined as wear. The parameters that affect wear are loads, speed, temperature, contact type, type of environment etc[31]. The wear is the loss of material and is expressed in terms of volume. Some of the common wear mechanisms are[26]:

1. Abrasion
2. Adhesion
3. Erosion
4. Tribochemical reactions
5. Surface fatigue
6. Cavitation
7. Fretting

Abrasion is when one body is in contact with another harder body and the surface peaks of the two bodies get broken[7]. Adhesive wear occurs due to localized bonding between the two mating surfaces leading to exchange of materials between them[25]. Erosion is the loss of material which occurs due to the impingement of a fluid containing solid particles on a surface. Surface fatigue occurs due to repeated stress caused by clearance size particles caught between the moving surfaces. Initially due to the impingement of solid particles on the surface, a crack is initiated. Then due to repeated stress, the crack propagates finally leading to failure of the material[32]. Tribochemical reactions are the chemical reactions which occur in tribological environment. Here, the

wear and the deformation are caused by the valency of the metal which causes them to react. Cavitation wear occurs due to imploding gas or bubbles entrained in the lubricant oil or hydraulic fluid[33]. Fretting occurs at the contact region between the two mating surfaces under load because of relative motion, vibration or some other force[34]. The relative motion leads to adhesive wear and the production of debris, this debris on oxidation causes abrasive wear at the point of contact leading to localized damage and losing of contact. Figure 1.1 shows some of the common wear mechanisms.

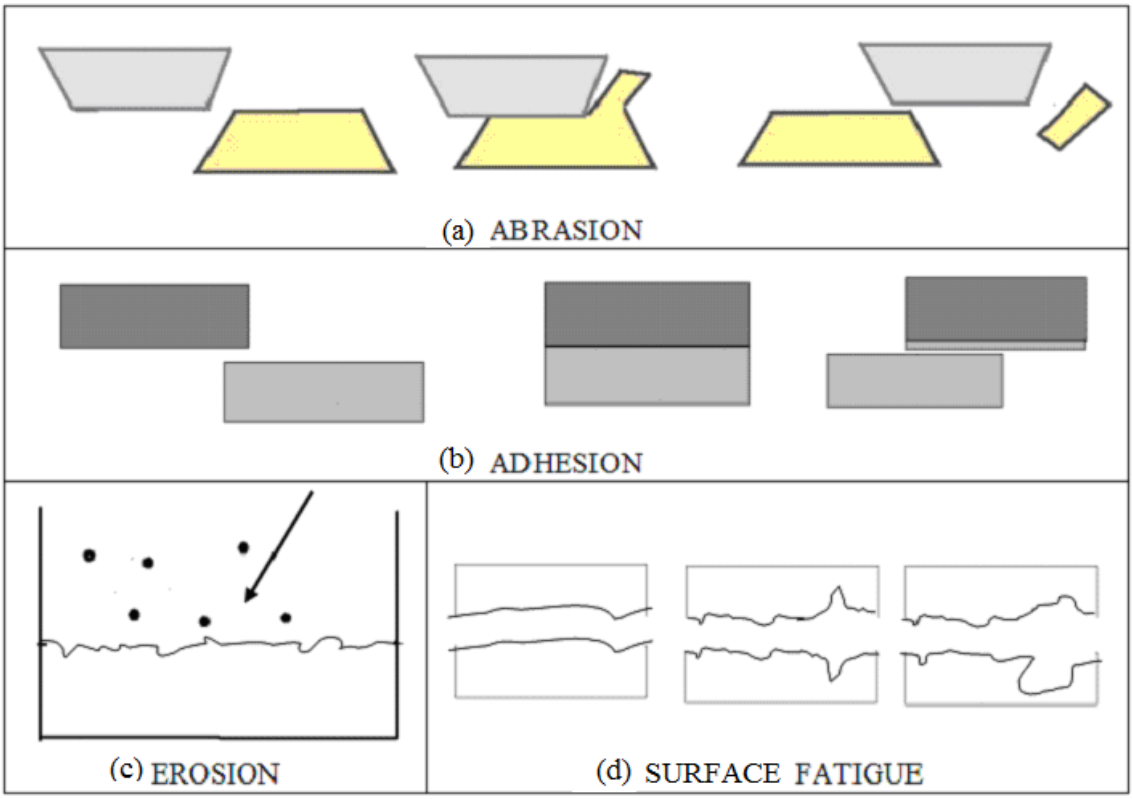

Figure 1.1 Different types of wear mechanisms: (a) Abrasion, (b) Adhesion, (c) Erosion, (d) Surface fatigue.

1.3.3 Lubrication

Lubrication controls the friction and wear by introducing a film between the contact surfaces in order to carry the load between the mating surfaces. Other than controlling friction and wear, it also helps to remove the wear particles and helps to cool the contact surfaces. Lubricants include oils, liquids such as water or emulsion and sometimes even gases. Lubrication can reduce the wear and thus increase the longevity. There are basically three modes of lubrication: boundary lubrication, mixed lubrication[7] and full fluid film lubrication[14] as shown in the figure 1.2.

These different modes of lubrication can be represented by a plot called the Stribeck plot which is usually used for studying the lubrication of journal bearings[35]. A typical Stribeck plot is shown in the figure 1.3. The Stribeck curve is plotted as the coefficient of friction versus the dimensionless Sommerfield number which is the product of viscosity and velocity divided by the load[36].

1. Boundary Lubrication mode: The boundary lubrication mode is the regime in which the load is carried by the surface asperity[37] as shown in the figure 1.2(a). The coefficient of friction is generally high since most of the friction is due to solid contact of the asperities as seen by the straight line in the figure 1.3.
2. Mixed Lubrication mode: Here the load is carried partly by the contact asperity between the two surfaces and partly by the lubricating fluid. The downward slope in the figure 1.3 indicates the mixed lubrication regime. The coefficient of friction decreases since the load is shared by the surface asperity and the lubricant[38]. This trend keeps on decreasing with the increase in the Sommerfield

number since there is less solid-to-solid contact with the increase in the Sommerfield number[39]. The intermittent contact leads to a lower coefficient of friction as compared to the boundary lubrication regime.

3. Full fluid-film lubrication mode: In the full fluid film lubrication regime there is no actual contact between the two mating surfaces and the load across the joint is carried by the lubricant entirely and there is no asperity contact[14]. Since the two surfaces are completely separated, the friction is controlled by the viscosity[15,16,17,18] and the shear rate rather than the surface asperities. The full fluid film lubrication regime shows an increasing trend with an increase in the Sommerfield number as shown in the figure 1.3.

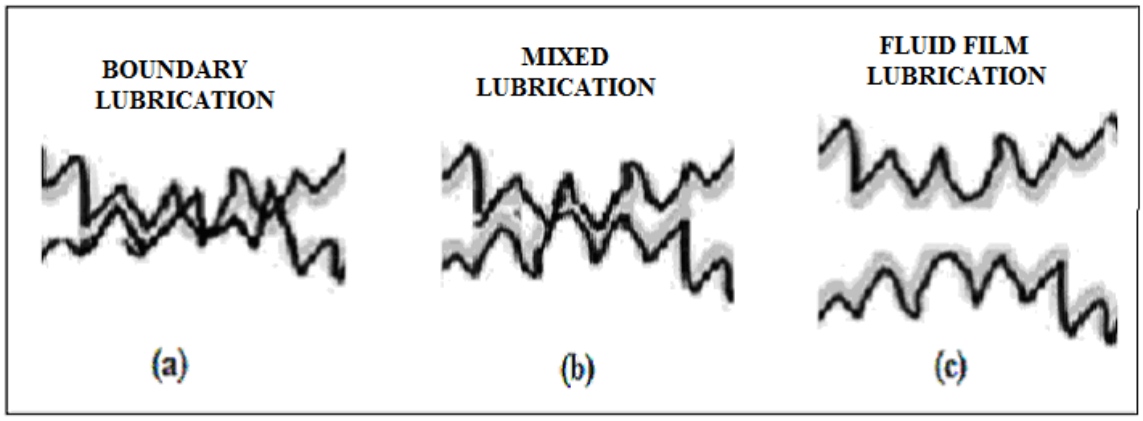

Figure 1.2. Different modes of lubrication.

This Stribeck plot can also be used to study the lubrication modes of the artificial joint[45], some of the examples found in the literature are shown in the figure 1.4. Thus, if the trend is going downwards then that indicates mixed lubrication regime whereas if the trend is rising then it indicates full fluid film lubrication regime[40,41].

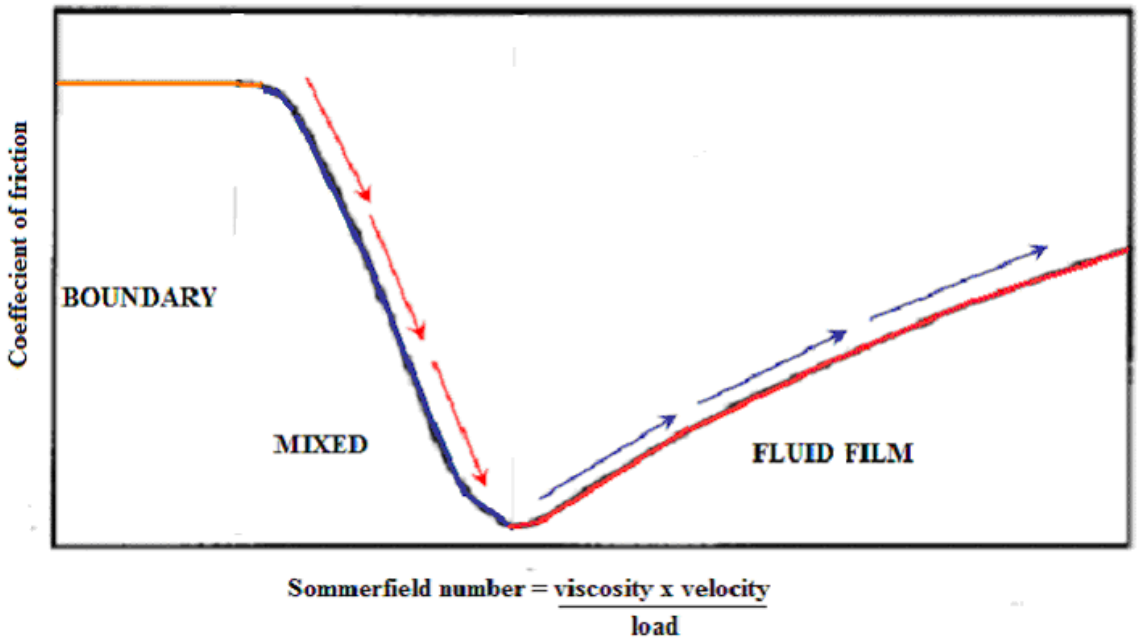

Figure 1.3. A typical Stribeck plot for journal bearings.

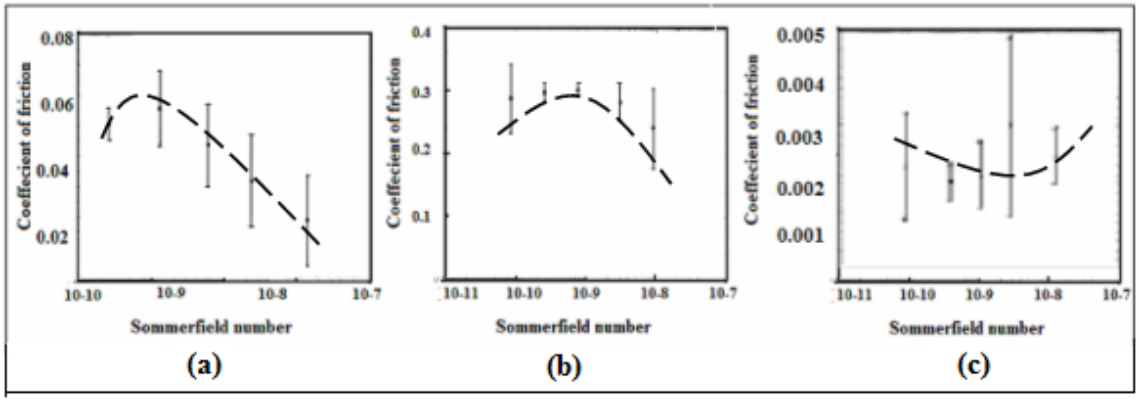

Figure 1.4. Stribeck plots for artificial joints[40,42,43].

Figure 1.4 (a) and figure 1.4 (b) shows a downward trend which indicates the mixed lubrication behavior whereas figure 1.4 (c) shows an upward trend which indicates full fluid film lubrication behavior.

1.4 Bio-Tribology

The word 'Biotribology' or 'bio-tribology' is not defined in the dictionary yet but it was first used in the year 1973 by Dowson and Wright. They defined biotribology as 'all aspects of tribology related to biological systems'. This definition is wide enough to encompass the tribology of all biological systems[44]. There are many examples of biotribology in the human body such as: wear of replacement heart valves[45], tribology of contact lenses and ocular tribology[46], lubrication of the heart in total artificial hearts[47], tribology in synovial joints and artificial replacements[48] etc. The main focus of this thesis will be the biotribology in synovial joints and artificial joint replacements. Thus, the tribological principles in friction, wear and lubrication as described above will be applied to solve the problems of artificial joint prostheses[49] to develop longer-lasting biomaterials and better lubrication.

1.4.1 Natural joints

Joints help us in movement by allowing the bones to articulate over one another. They are a crucial component not only for humans but also in animal locomotion and motion at the cellular level. Their proportions differ depending upon the location and the function of the joint[50].

Depending upon the degree and the type of movement that they allow, joints can be classified as[51]:

1. Fibrous (or Immovable) Joints: These joints, called the synarthroses, exist in the body where the movement is minimal. These joints are held together by a thin

layer of strong connective tissue[52]. e.g., different bones of the skull, teeth in the socket etc.

2. Cartilaginous Joints: These joints, called amphiarthroses, allow only a slight movement. These bones are joined together by white fibro-cartilaginous discs and ligaments which restricts the movement[53]. e.g., Tibia and Fibula of the leg, Ulna and Radius of the arm etc.
3. Synovial Joints: These joints also called diarthroses, allow full and free movement. Most of the joints in the human body are of this type[53]. e.g., hip joint. knee joint, shoulder etc.

Since the synovial joints are the only joints in the body which permit full motion. They are the only joints in which the effects of friction, wear and lubrication can be observed.

1.4.1.1 Synovial joints

The synovial joints are so called because of the synovial fluid present in the joint. They allow free movement in the body. Even the small ossicles in the ear, which is the smallest bone in the body, is a typical synovial joint. The structure of a typical synovial joint is shown in the figure 1.5. Its main parts are: articulating capsule, articulating membrane and synovial fluid[53].

1. Articulating capsule: This capsule surrounds the articulating bones and acts as a seal. It has two layers: external fibrous capsule and the internal synovial membrane.

a. Fibrous capsule: It is made of strong connective tissue which holds the two bones together and prevents their dislocation during normal movement.

b. Synovial membrane: It is present along the inner surface of the articulating capsule and forms a sac-like structure which holds the synovial fluid. Its inner layer has special cells which produces the synovial fluid[54].

2. Articular cartilage: The ends of both the articulating bones are covered with a smooth cartilage so that the bones do not come in contact with each other. It is about 2-3 mm thick and can withstand a pressure of 1-4 MPa about 200 million times a year without separation from the bone[55]. It does not have blood supply and is nourished by the synovial fluid[56].

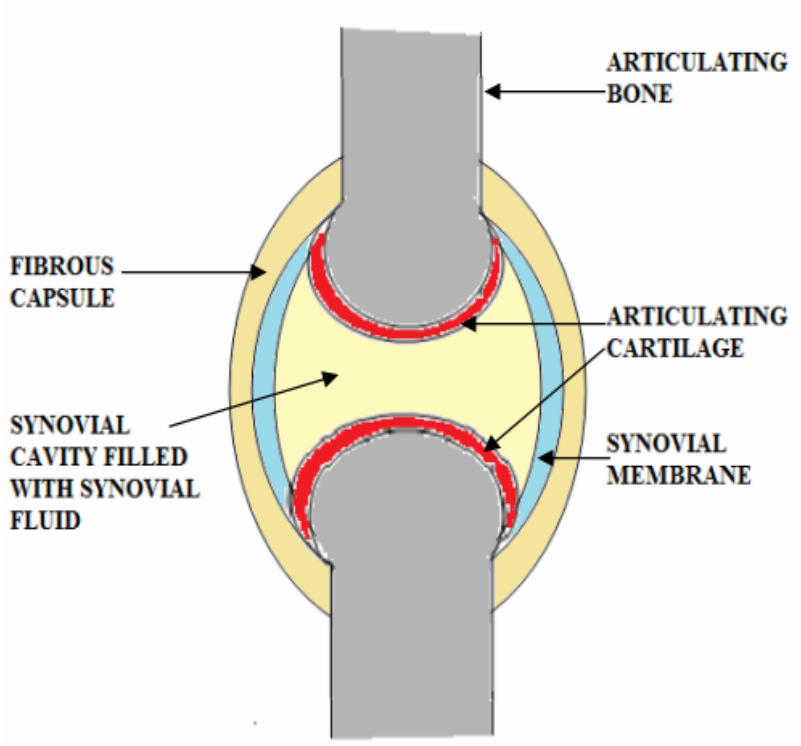

Figure 1.5. A typical synovial joint.

3. Synovial fluid: The synovial fluid is the nourishing fluid rich in mucopolysaccharide which makes it thick and viscous. It has two main functions: to lubricate the two articulating surfaces, and to distribute the nutrients and remove the wastes[51.] Large synovial joints e.g. knee usually have about 3 ml or less of Synovial fluid[55]. The movement of the joint helps to circulate the synovial fluid continuously. Thus the cartilage and the synovial fluid together keep the friction low by keeping the joint lubricated hydrodynamically[57]. The synovial fluid lubricates the joint with an effect called the 'squeeze effect' wherein the film becomes thinner during loading and becomes thicker during unloading[50].

The synovial joint may also have many other accessory structures depending upon the type of joint and its function. These accessory structures help to strengthen and stabilize the joint. They could be in the form of additional ligaments, cartilages, fat, tendons etc.[54]

1.4.2. Joint malfunction

Joints in the body are susceptible to failure. All of the above mentioned different types of synovial joints irrespective of the type and function can fail. They may fail due to many reasons such as accidents, illness, arthritis, over-use, old age, trauma, etc. Accidents may damage the hyaline cartilage, which can regenerate itself as a fibrocartilage but it will have poor wear resistance[58]. Arthritis is of many types: osteoarthritis, gout, Fibromyalgia, rheumatoid arthritis, bursitis, etc and can lead to loss

of joint function[59]. Arthritis comes from Greek words ‘arthro’ meaning ‘joint’ and ‘itis’ meaning ‘inflammation’ therefore arthritis means ‘inflammation of the joints’[60].

In short, a combination of many chemical, mechanical and biological factors lead to development of pain, stiffness and finally loss in the free movement of the joint. There are three main methods of treatment:

1. Painkillers or analgesics[61]
2. Steroids[62]
3. Joint prostheses.

The doctor will always try the first two modes of treatment and then only consider surgery. Joint prosthesis is a more popular mode of treatment since it relieves pain, improves quality of life and helps people get back to normal life. Total joint replacements are possible for hip, knee, ankle, shoulder, elbow, wrist, thumb and finger joints.

1.4.3. Joint prosthesis

Joint prosthesis as mentioned above is possible for many synovial joints, but we will be focusing on hip joint replacement since among all the joint replacements it is the most common one. Since the initial success a lot of research has been done in the tribology of natural and artificial joints[40,44,50]. Here, the articulating bones get damaged and they are either replaced or covered by artificial bearing couples. The bearing couples that are generally used are: plastic-on-metal, metal-on-metal or ceramic-on-ceramic, some other combinations such as metal and highly cross-linked polymer or ceramic and

highly cross-linked polymer are also available[63]. All of these bearing pairs have their own strengths and limitations. The choice of either of this implant depends upon many factors such as age, activity level, weight, component design, health and the choice of the orthopedic surgeon. Young people need more wear resistant and longer lasting hip prosthesis to reduce the possibility of revision surgery[64].

For example in the case of hip replacements, part of the thigh bone (femur) with the ball is removed and an artificial ball is fixed to the rest of the thigh bone. The surface of the socket in the pelvis is made rough and a new artificial socket is inserted in the pelvis which will join with the ball component. Figure 1.6 shows a healthy hip, an arthritic hip and artificial hip replacement.

Most artificial joints are joined with acrylic cement but in active patients sometimes one or even both the parts are inserted without the cement[65]. In the latter case, the implants are roughened so that the bone will grow onto them which will provide a much better and a longer-lasting bond.

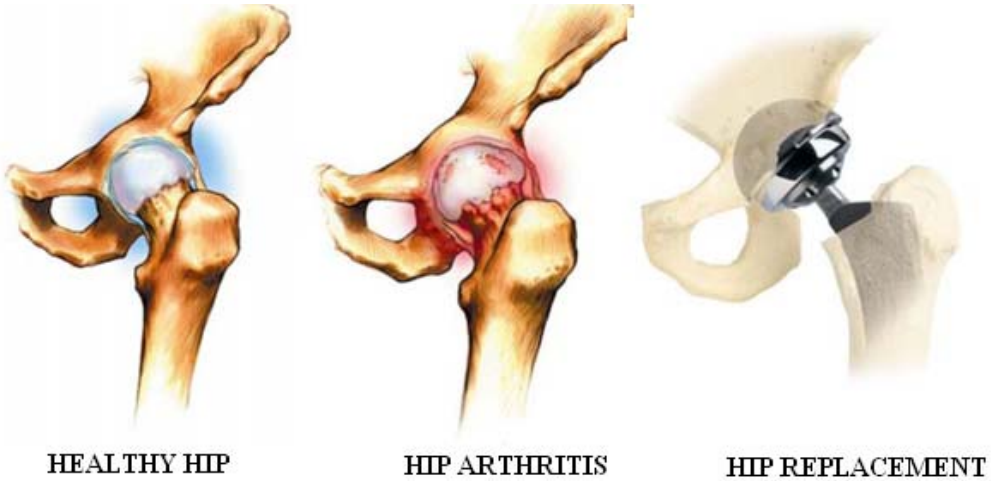

Figure 1.6. A healthy hip, arthritic hip and a hip replacement[66].

1.4.3.1 Plastic-on-metal implant

Here the ball and the socket both are made up of metal prosthesis but a plastic spacer is placed in between them. Figure 1.7 shows a typical plastic-on-metal hip joint. It has a plastic insert and the metal rubs on the plastic and so it is called plastic-on-metal. The metals usually used are: titanium, stainless steel and cobalt chrome, and the plastic is polyethylene. Now the plastic is replaced with ultra-high molecular weight polyethylene (UHMWPE). UHMWPE has been more successful in reducing the friction and wear at the joint, thus producing less wear debris. This implant can be attached to the bones either by press-fit or by using bone cement.

But the biggest drawback is the production of plastic debris which causes osteolysis leading to aseptic loosening of the joint[67]. Osteolysis is the resorption or dissolution of the bone tissue. Initially this phenomenon was attributed to the cement used for fixation, but later it was discovered that it was due to the polyethylene wear debris. Aseptic loosening i.e. loosening not related to any infectious process, is the biggest cause for revision surgery.

The size of the polyethylene debris is usually in the range of 0.1-0.5 μm[68] and the critical accumulated wear volume of UHMWPE beyond which loosening starts is 508 mm^3 for cemented joints[69] and 551 mm^3 for cementless joint[70].

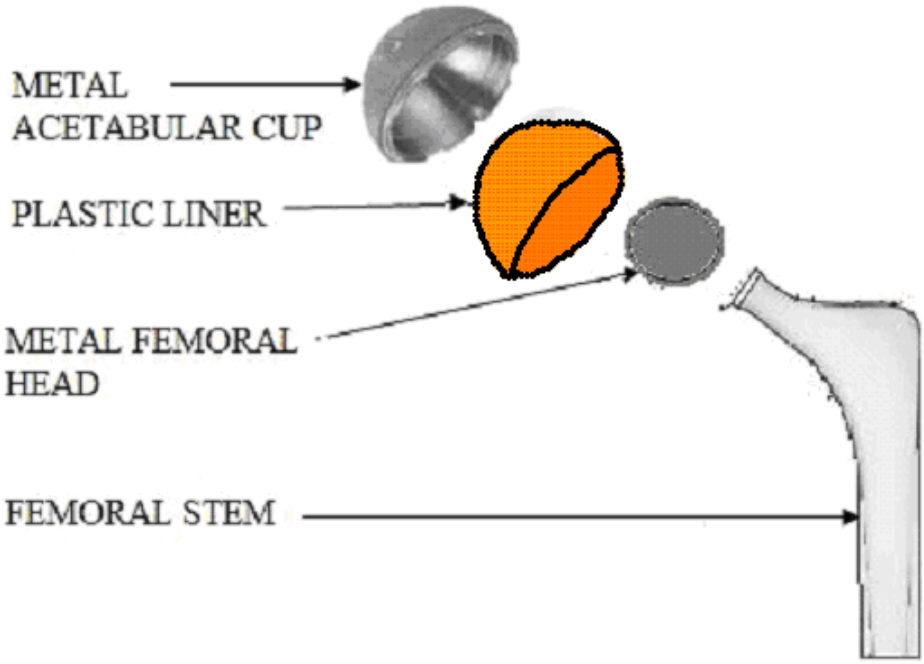

Figure 1.7. A typical plastic-on-metal hip joint.

1.4.3.2 Metal-on-metal implant

In metal-on-metal implant the two articulating bones are covered with the metal prosthesis, similar to the plastic-on-metal but there is no plastic spacer in between them. It was used 30 years ago but it failed due to the poor manufacturing technique, now with the development of harder and smoother metal the metal-on-metal hip implants have shown a 99% reduction of volumetric wear as compared to the plastic-on-metal[71]. Figure 1.8 shows a metal-on-metal hip joint. Also many times instead of removing the ball of the Femur bone completely, an artificial cap is fitted onto the ball, but this technique cannot be used for people suffering from osteoporosis or those who have low density bone.

The size of the wear debris particles from the metal-on-metal prosthesis are found to be between 0.015-0.025 μm[72]. Since the metal debris produced is of relatively small size, thus a small volume of metal wear will produce a lot of wear debris particles as compared to the plastic debris, but the biological effect of these particles is relatively less than the plastic debris[73]. The metallic wear debris or ions get systematically distributed in the body and have been observed to be found in the lymphoreticular tissues[74], blood and urine[75] and these metallic ions causes lymphadenopathy[76] and necrosis[77].

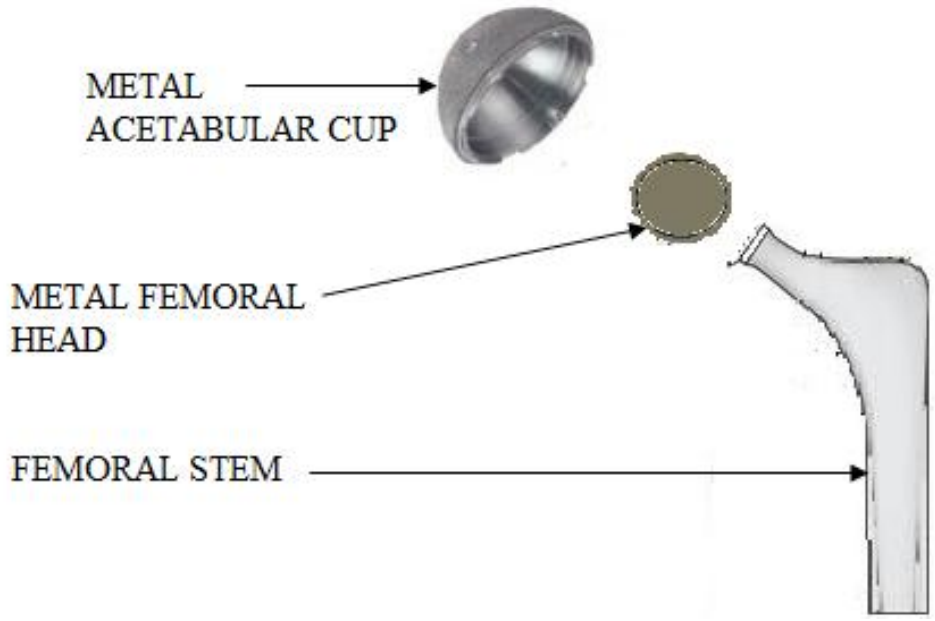

Figure 1.8. A typical metal-on-metal joint.

1.4.3.3 Ceramic-on-ceramic implant

For the ceramic-on-ceramic joint the bearing pair is made of a ceramic material. The ceramics that can be used are Zirconia, Alumina etc. Ceramics are more scratch

resistant, harder and smother than the other metals and plastics, thus they exhibit lower coefficient of friction, lower wear and better lubrication. They not only demonstrate lower wear but also lower biological reactivity as compared to any other bearing pair[78]. They don't show any significant ion release or corrosion rate[79]. The socket can be made small providing easier and more flexible movement without the chances of dislocation. Also harder material will provide better lubrication and so there will be less wear.

The main reason which has led to so much interest in ceramic-on-ceramic joints is due to the hardness of the ceramics as compared to the other materials. A general wear equation is[80]:

$$\text{Volume} = klx/3p$$

K = probability of producing a wear particle x = sliding distance

L = normal load p = hardness of the softer material

Thus on increasing the hardness, the wear volume will reduce. Thus, these implants are expected to be longer lasting than the other bearing pairs.

In the present research, we tested MAO alumina (ceramic) coatings for its potential use as a biomaterial.

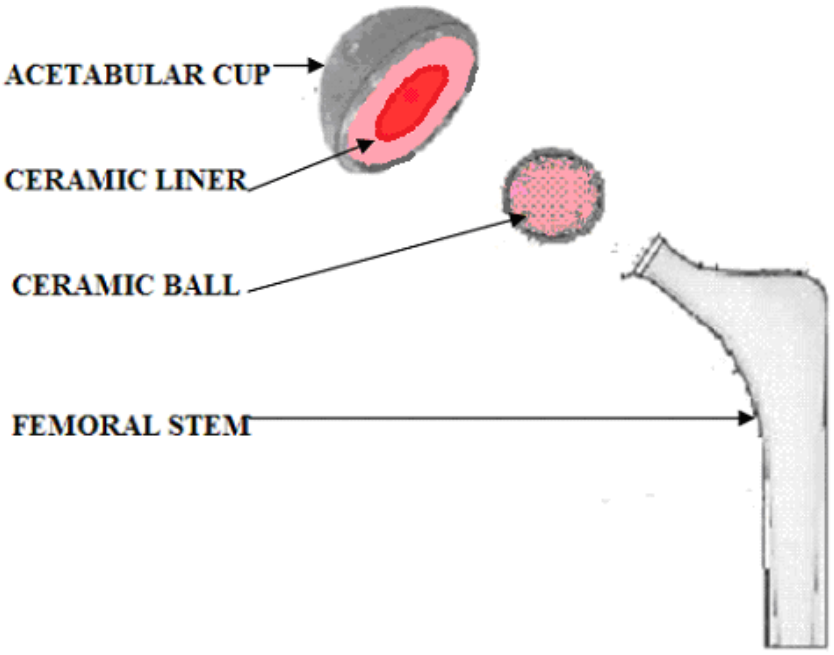

Figure 1.9. A typical ceramic-on-ceramic joint.

1.4.4 Joint lubrication with nanoparticles

1.4.4.1 Need for lubrication

The main problems causing failure of artificial joints are: mechanical loosening, infection, fracture, instability, wear, inadequate lubrication[81]. Out of all these causes, inadequate lubrication is one of the primary reasons for joint failure[81]. Also in the case of osteoarthritis, the articular cartilage disintegrates and the synovial fluid present in the joint loses its viscosity leading to joint stiffness and pain. Series of injections have then to be taken to increase the shock absorbing capacity of the Synovial fluid. Thus lubrication plays a very vital role in the easy and flexible movement of the joint.

1.4.4.2 Why nanoparticles?

Nanoparticles have a very high surface-to-volume ratio leading to many unique and advanced properties as compared to the bulk material[82]. It has been studied that the nanoparticles have a great potential in the field of tribology as additives to the lubricant. Success of any additive in a lubricant depends on the particle size[83]. Addition of nanoparticles has shown to increase the friction resistance[81], wear resistance[84] and the load bearing capacity of engine oil[85]. This is because the nanoparticles embed themselves in the small asperity of the surface and thus prevent the two surfaces to meet which reduces the wear at the contact surfaces. Also in the lubricant, these nanoparticles act as ball bearings rubbing against each other and thus preventing the two surfaces from interacting. Nanoparticles of many materials such as copper[86], MoS_2[87], palladium[82] etc have proven to have better anti-wear and load bearing capability than the conventional lubricants such as ZDDP available in the market. Use of silver nanoparticles in UHMWPE have shown reduction in wear and increase in the biocompatibility and antimicrobial activity[88].

In the present research we propose to add gold nanoparticles to the bovine calf serum to study their effect on lubrication for its potential use in biomedical applications.

1.5 Remarks

As discussed in this section, friction, lubrication, and wear play a vital role in human bodies. Synovial joints such as hip, knee, shoulder etc, are, in particular, of great interest in biotribology since they permit full and free movement. The functions of these joints sometimes get affected and from all the modes of treatment available, artificial joint replacement is the best mode of treatment since they not only relieve pain but also increase mobility. The natural joints are lubricated by the synovial fluid and so the coefficient of friction obtained in these joints is low resulting in low wear whereas the coefficient of friction obtained in the commercial implants is very high and the consequent wear is very high thereby limiting the life span of these artificial joints to only 10-15 years[89]. Also in the case of osteoarthritis, a form of arthritis, the synovial fluid breaks down reducing the shock absorbing capacity of the synovial fluid leading to pain and stiffness of the joint. Synthetic biofluid is then inserted in the joint in the form of series of injections which improves the lubrication in the joint by increasing the shock absorbing capacity of the synovial fluid and helps in relieving pain but they only work for 6-9 months after which the cycle has to be repeated.

The number of people needing artificial joint implants is estimated to be nearly 43 million people in United States alone which is estimated to rise to 60 million by the year 2020[90]. With the increasing number of people needing these artificial joints, it has thus become imperative to develop newer and better materials for artificial replacements and lubrication.

2. MOTIVATION AND OBJECTIVES

As discussed in section 1, the lifespan of artificial joints needs to be increased. For doing so, the first step is to gain a basic understanding of biotribological principles of biomaterials. The properties required for the success of any biomaterial in artificial joint prosthesis are biocompatibility, high hardness, good wear resistance, good fracture strength etc. With the advancement in the coating technology, newer and better coatings with improved mechanical properties such as hardness, corrosion resistance, load bearing capacity, and adhesion strength are being developed. These coatings could be potentially used to synthesize artificial joints which would be longer lasting and exhibiting lower wear and friction.

Nanoparticles with their high surface-to-volume ratio have been used as additives in lubricants to increase the anti-wear and load bearing capacity of the lubricant. They adhere to the surface asperities and prevent the two surfaces to interact, improving the lubrication.

This thesis has two research objectives, mainly to obtain understanding in new coatings and fluid lubrication.

1. Develop basic understanding in microstructure-property relationship of new materials and coatings. We will firstly seek new biomaterials and coatings through tribological evaluation and subsequently find potential for their use in artificial joints. To that end, Micro Arc Oxidized (MAO) alumina (ceramic) coatings at different current intensities were studied.

2. Develop biofluids which would improve the lubrication properties. We propose to use nanoparticles to modify synthetic biofluids and study their interfacial interactions under tribological conditions. The effects of nanoparticles, their concentration and shape, will be studied.

The knowledge developed here will be beneficial for the design of new biomaterials as well as the improvement and the development of better and longer lasting artificial joints. The design methodology developed here for biomaterials and biofluids will lead to reduction in the joint pain and increased mobility of the joint.

3. EXPERIMENTAL PROCEDURE

This section deals with the materials, tribology and surface characterization tools, and the experimental procedure used to test the alumina (ceramic) coatings for its feasibility as an implant material, and for the lubrication studies using different concentration and shape of gold nanoparticles.

3.1 Materials

To characterize the ceramic coatings the materials used were:

3.1.1 Micro Arc Oxidized (MAO) alumina coatings

3.1.2 Silicon nitride

3.1.3 Synthetic biofluid

For the lubrication studies, the materials used were:

3.1.4 Gold nanoparticles

3.1.5 Bovine calf serum

3.1.6 Egg

3.1.1 Micro Arc Oxidized (MAO) alumina coatings

Rectangular samples of aluminum alloy Al-7039 T6 were used as substrates; the nominal composition of this alloy is 0.068 % Si, 0.139% Fe, 0.081% Cu, 0.266% Mn, 2.25% Mg, 0.198% Cr, 4.12% Zn, 0.012% Ti and Al balance. A ‘Microarc Oxidation’ (MAO) method was used to generate the alumina coatings.

The principle of Microarc Oxidation method is anodic polarization in aqueous electrolyte solution with plasma discharge on the anode. Once the critical value of the polarization potential is exceeded then numerous plasma discharges occur over the entire surface. This method is a combination of electrochemical oxidation and high voltage spark treatment and thus the coating has excellent physiochemical properties[91]. Because of the high temperature and pressure reached[92], oxide based layers are formed on the anode surface which have improved mechanical properties such as hardness, adhesive strength, load bearing capacity, corrosion resistance as compared with other coatings[93].

The MAO coatings were produced using a 100 kW Micro-Arc Oxidation (MAO) equipment, consisting of a stainless steel container, an AC power supply, cooling and stirring systems. Figure 3.1 shows the experimental setup used to generate these coatings. The Al alloy specimen was the anode and the wall of the stainless steel container was the cathode. A solution of 9.5 g/l $Na_2SiO_3.5H_2O$ and 2 g/l KOH in distilled water was used as the electrolyte and its temperature was controlled to remain lower than 35°C during treatment.

MAO Alumina coatings were produced at different current densities such as 0.100 A/cm^2 0.125 A/cm^2, 0.150 A/cm^2.

The three layers obtained in the coating are shown in figure 3.2. The external layer is relatively porous as can be seen from the voids and cracks seen in the layer and thus less hard. It is followed by a dense internal region which is very thick and non-porous and thus hard. Lastly there is a thin interfacial layer which separates the coating and the substrate.

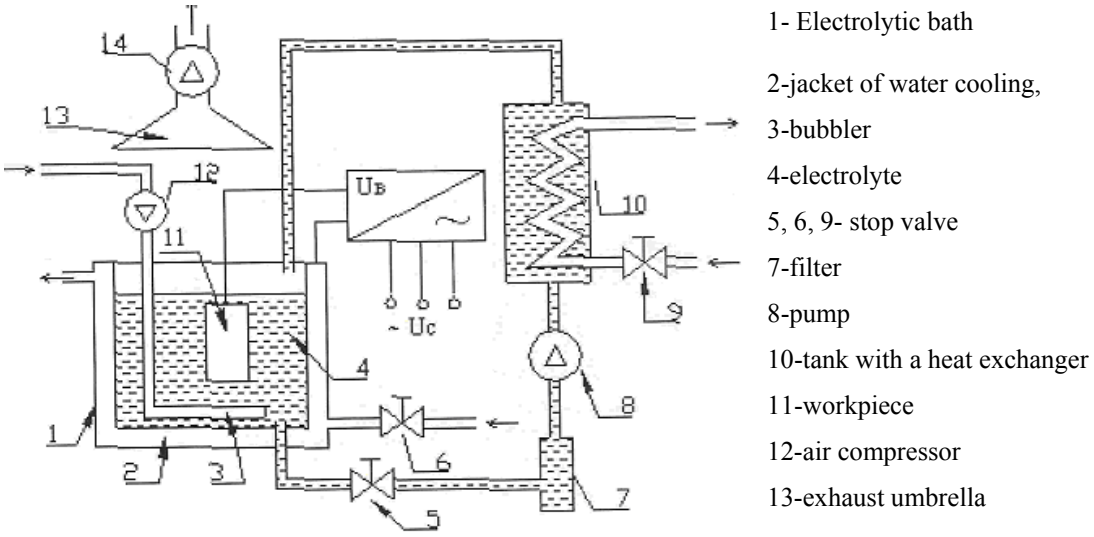

Figure 3.1. Experimental setup used to generate the MAO coatings.

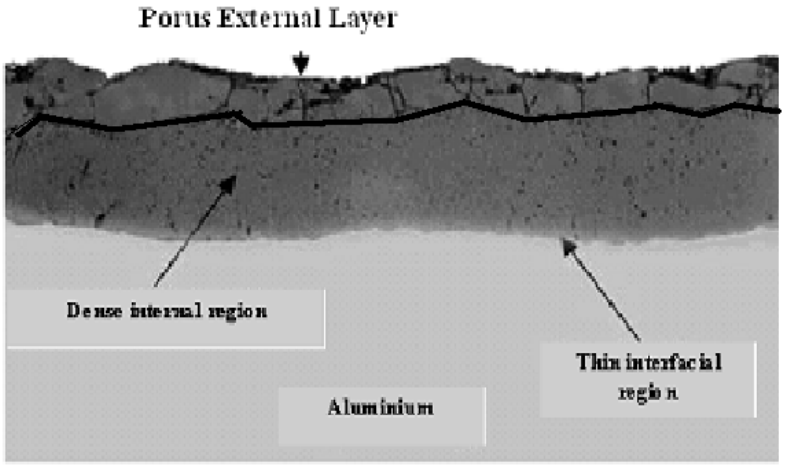

Figure 3.2. Different layers of the coating.

The different characteristics of the coatings: thickness, hardness, microstructure and surface roughness, were analyzed. The coating thickness was measured using an eddy current coating thickness measurement gauge (Fisher, Germany). The hardness of the coatings was evaluated by a scratch test on a pin-on-disk tribometer (CSM instruments). The microstructure was studied using a scanning electron microscope

(JEOL) and the surface roughness was measured using a profilometer (Veeco Dektak, Sloan Technology). The results obtained are tabulated in table 3.1.

Table 3.1
Coating thickness, hardness, microstructure and surface roughness of the three MAO coatings

Coatings	***Coating Thickness (μm)***	***Scratch Test (N)***	***Micro-structure***	***Surface Roughness (μm)***
0.100 A/cm^2	96.20	0.735	Aluminium, Mullite, δAl_2O_3, Al_2O_3	7.53
0.125 A/cm^2	128.0	0.760	Aluminium, Mullite, γ Al_2O_3	8.59
0.150 A/cm^2	142.0	0.845	Mullite, γ Al_2O_3, α Al_2O_3, Al_2O_3	9.59

The hardness of any coating depends on its constitutive phases. The microstructure of these coatings shows the presence of Mullite, γ Al_2O_3, α Al_2O_3, Al_2O_3, and Aluminium. Mullite is a mixture of Alumina and silica. The maximum hardness value for the α-Al_2O_3 phase is 17 to 22 GPa and for γ- Al_2O_3 it is 10 to 15 GPa. From table 3.1, the 0.150 A/cm^2 coatings has both the α-Al_2O_3 and γ-Al_2O_3 phases and thus will be the hardest amongst all the three coatings, followed by the 0.125 A/cm^2 coating containing only the γ-Al_2O_3 phase and finally the 0.100 A/cm^2 coating, which does not

contain either the α-Al_2O_3 or the γ-Al_2O_3 phase. This result is validated from the scratch test used to determine the hardness of the three coatings.

3.1.2. Silicon nitride

A silicon nitride ball of 6 mm diameter was used as the corresponding sliding partner. Silicon nitride, a ceramic was chosen against the alumina coating to simulate the ceramic-on-ceramic joint. It had 94.2% beta-phase (Norton NBD 200), was isostatically hot pressed, and had a surface finish of around 0.1 μm. Silicon nitride was selected as the partner since it exhibits very high resistance to heat and corrosion and is an unusually strong ceramic.

3.1.3 Synthetic biofluid

SBF (Synthetic Biofluid) was supplied by Lynntech Inc. It was buffered at a pH of 7.25 with Tris (hydroxymethyl) aminomethane and HCl. The ionic concentrations in SBF are given in table 3.2.

Table 3.2
Ionic concentrations in synthetic biofluid

Ions	***Concentration (%)***
$\mathbf{Cl^-}$	48.5
$\mathbf{Na^+}$	46.6
$\mathbf{K^+}$	1.6
$\mathbf{HCO^{3-}}$	1.4
$\mathbf{Ca^{2+}}$	0.82
$\mathbf{Mg^+}$	0.5
$\mathbf{HPO^{4-}}$	0.33
$\mathbf{SO_4^{3-}}$	0.16

3.1.4. Gold nanoparticles

Gold has been used since ancient times because of its stability and biocompatibility. The use of gold in dentistry is well known. Gold water, made by boiling a gold nugget in water has been used for centuries for a variety of illness. It is said to act as an anti-inflammatory and has been used as a supplement to aspirin for pain relief during arthritis[94]. Thus gold was chosen and different shapes of nanoparticles such as: spherical and rods were used.

Deep red solutions of colloidal gold were prepared by Michael Faraday in the mid-nineteenth century by the reduction of chloroaurate [$AuCl_4^-$] solutions using phosphorus as a reducing agent[95]. The particles in their nano regime i.e., in their 'neglected dimension' exhibit special properties in many aspects compare to the bulk

properties. e.g., catalysis[96,97,98,99], size and shape dependent optical properties[100], electronic properties[101], medicinal applications[102], applications in optical devices[103] etc. But to reach from bulk state to nanoscale has been a challenge. In recent years, it has become possible to investigate the size dependent nature of chemical and physical properties in the nanoscale regime[104]. But the stabilization of these particles has been more difficult due to particle agglomeration/aggregation because at short inter-particle distance, two particles would be attracted to each other by Van der Wall forces and in the absence of repulsive forces to counteract this attraction an unprotected solution would coagulate. This counteraction can be achieved by two methods, electrostatic stabilization and steric stabilization. For example, during preparation of gold solution by the reduction of aqueous [$AuCl_4^-$] by sodium citrate, the colloidal gold particles are surrounded by an electrical double layer formed by adsorbed citrate and chloride ions and cations, which are attracted to them. In all cases some stabilizer like micelle[105], thiol[106], dendrimer[107] or polymeric ligands[108,109] or some sulfur/nitrogen containing ligands are needed to prevent the colloidal particles from aggregation by providing a protective layer.

Here, we prepared spherical and rod shaped gold nanoparticles using a positively charge surfactant CTAB and seeding growth approach.

3.1.4.1 *Spherical nanoparticles*

Spherical shaped or nanospheres were synthesized by preparing gold seeds, which were obtained by reducing 1 ml. of 10 mM $HAuCl_4$ with 1 ml. of 100 mM $NaBH_4$

in the presence of 1 ml. of 10 mM sodium citrate and 36 ml. of DI water. The resulting seed mixture was aged for 2-4 hours in order to allow the hydrolysis of the unreacted $NaBH_4$. These gold nanoparticle seeds exhibited a plasmon resonance peak at 500 nm and had an average diameter of 5.2 ± 0.6 nm.

The third solution contained 2.5 ml. of 10 mM $HAuCl_4$, 0.50 ml. of 100 mM NaOH, 0.50 ml. of 100 mM ascorbic acid and 9 ml. of CTAB solution. Nanoparticle formation with large diameter was initiated by adding 1 ml. of seed solution to growth solution 1. After 5 minutes, 1 ml. of resulting mixture was added to growth solution 2 and then after 5 minutes all of the mixture was added to growth solution 3. This solution was then centrifuged at 8000 rpm for 20 minutes to remove the excess CTAB and the precipitated gold nanoparticles were redispersed in DI water. Figure 3.3 shows the size and shape of the nanoparticles obtained.

As can be seen from the Figure 3.3, the nanoparticles were almost homogeneous, having spherical shape and a diameter of around 40-50 nm and well dispersed in the CTAB solution. The CTAB forms a micelle in the aqueous solution by disintegrating into CTA^+ and Br^-. The Br^- is released in the solution and the CTA^+ adheres around the nanoparticle keeping them from aggregating. This CTA^+ around the nanoparticle gives it its positive charge. Figure 3.4 shows a pictorial representation of the surfactant molecule around the nanoparticle.

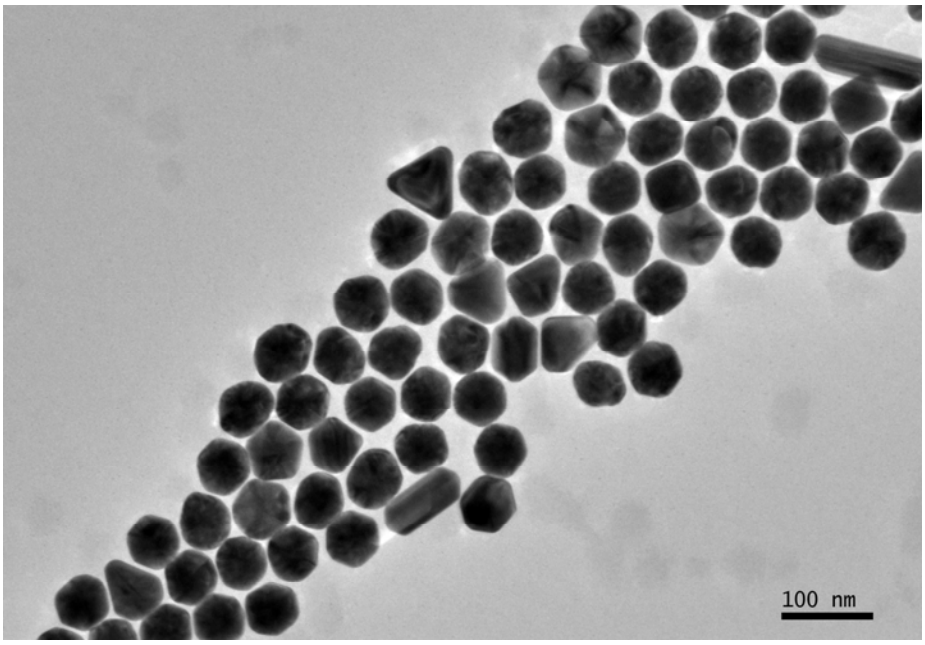

Figure 3.3. TEM image of the spherical gold nanoparticles.

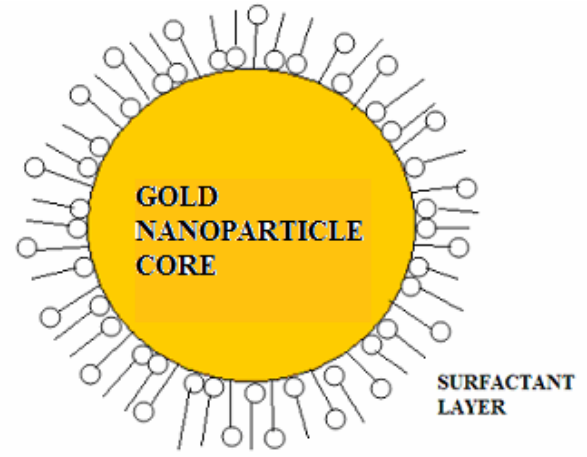

Figure 3.4. Surfactant layer of CTAB around the gold nanoparticles.

3.1.4.2 Rod-shaped nanoparticles

Rod-shaped gold nanoparticles or nanorods were synthesized by the three-step seeding growth techniques as described previously. Specifically, two 20 ml conical

flasks (named A & B) and one 100 ml conical flask (leveled C) were taken. Three growth solutions were prepared each containing a mixture of 2.5 x 10^{-4} M $HAuCl_4$ and 0.1 M CTAB solution. To these solutions were added 50 µl (flasks A and B) and 250 µl (flask C) of 0.1 M freshly prepared ascorbic acid, and the resulting solutions were stirred gently. The orange color of the gold salt in the CTAB solution disappeared when ascorbic acid was added leading to the reduction of Au^{3+} to Au^{+}. However, further reduction of Au^{+} to Au^{0} occurs when 1.0 ml of the seed solution is mixed with sample A (step 1). After 15 seconds, 1.0 ml. of sample A was mixed with sample B (step 2). A 5.0 ml portion of sample B was further added to sample C after 30 seconds (step 3).

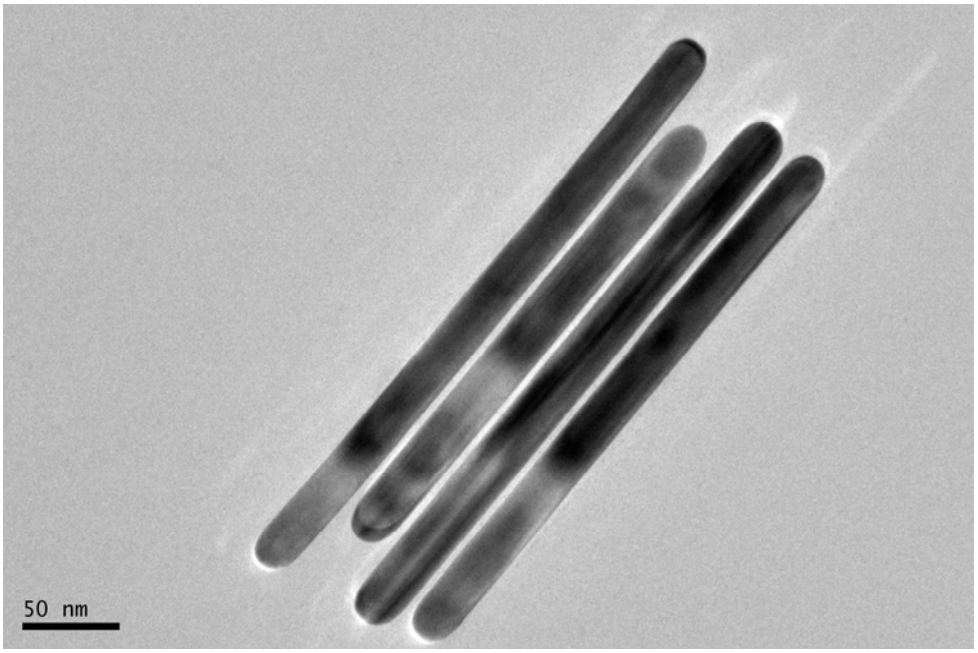

Figure 3.5. TEM image of the rod-shaped gold nanoparticles.

The color of this solution slowly changed to purple. In all steps, the flask was gently stirred to homogenize the solutions. The solution in flask C was kept at 25 °C for

a period of 16 hours. To obtain gold nanorods, purification is required. All the top red-brown solution (which contains mostly spheres) was slowly removed by suction. A faint brown tinge can be observed at the bottom of the flask. 5.0 ml of DI water was flushed into the beaker, and the contents were agitated for some time. A greenish-brown color developed in the DI water which intensified upon repeated agitation. The solution now obtained contained a high percentage of gold nanorods, though other shapes (triangles, hexagons, and small rods) were also present in small amounts. The excess CTAB was removed by centrifugation (at 7000 rpm) and washed with DI water. Figure 3.5 shows the rod-shaped nanoparticles obtained using the seed mediated approach.

3.1.5 Bovine calf serum

Bovine Serum was obtained from Hyclone Inc. (Thermo Fisher Scientific). Bovine serum is processed calf blood which is used in research to simulate the bodily conditions. The Biochemical assay of the bovine calf serum is given in table 3.3[110]. As seen in the table, the serum contains proteins, enzymes and metals. The serum was buffered at a ph of 7.33.

The serum was stored at -10° C or lower. For the experiment, the serum was transferred to a water bath at 37° C and was agitated periodically so that the solutes were not concentrated at the bottom of the container. Care was taken such that the temperature did not exceed 40° C so as to cook the proteins. Figure 3.6 shows the TEM image of the air-dried serum. Bovine has been reported as a promising biofluid[64] and comes closest to synovial fluid. Thus we used the same to study the effect of nanoparticles on lubrication

properties of the biofluid. Subsequently, different concentrations of nanoparticles were mixed with the bovine serum to produce the solution at different concentrations of 25%, 50% and 75% of nanoparticles.

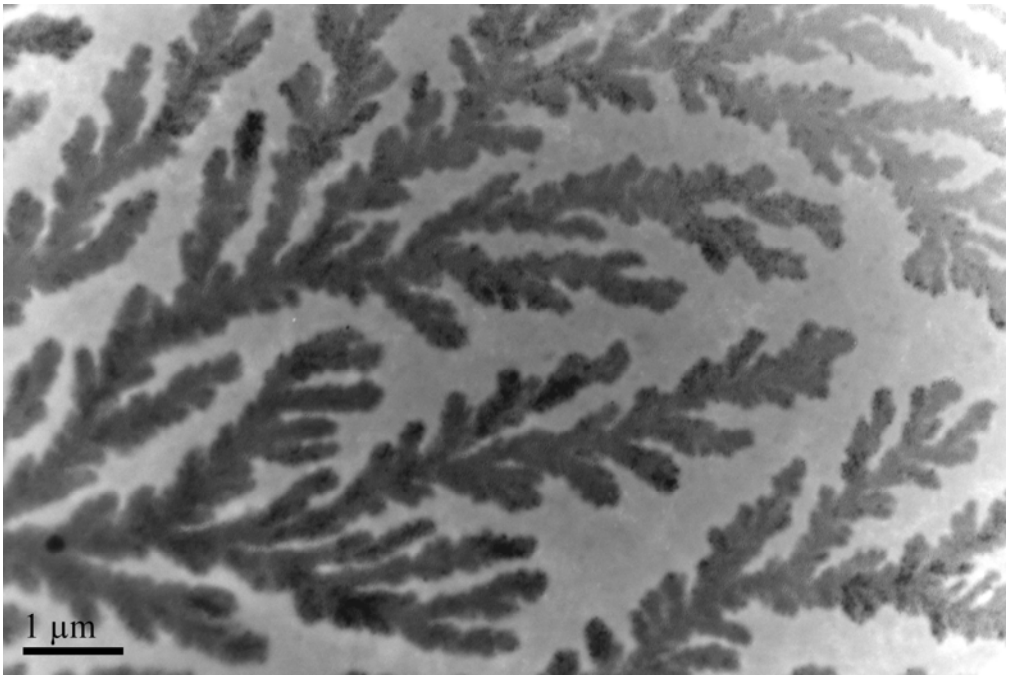

Figure 3.6. TEM image of the air dried bovine calf serum.

Table 3.3
Biochemical Assay of bovine calf serum

PROTEINS/OTHER	
Albumin	3.2 gm%
Alkaline Phosphatase	225 mU/mL
Blood Urea Nitrogen	5 mg/dL
Creatinine	1.3 mg/dL
Gamma Globulin	12.8 % tp
Glucose	81 mg/d
Glutamic Oxaloacetic Transaminase(SGOT)	134 mU/mL
Glutamic Pruvic Transaminase (SGPT)	41 mU/mL
IqG-Nephelometer	14.5 mg/mL
Lactase Dehydrogenase	4820 mU/mL
Osmolality	296 mOsm/Kg
Total Bilirubin	0.4 mg/dL
Total Protein	6.9 gm%
TRACE METALS/IRON	
Calcium	10.9 mg/dL
Chloride	101 mEq/L
Inorganic Phosphorus	9.1 mg/dL
Iron	469Ug/dL
Percent Saturation (Iron)	81 %
Potassium	6.0 mEq/L
Sodium	142 mEq/L
Total Iron Binding Capacity (TIBC)	581 ug/dL

3.1.6 Egg

Serum is composed of many proteins, enzymes, and elements as seen in table 3.3. In order to study the interaction of nanoparticles with a protein, egg white was used for comparison purpose. Egg white contains the protein albumin which is used to nourish the growing embryo. Thus, the tribology tests were conducted with egg albumin and nanoparticles to understand the nanoparticle-protein interaction which would be beneficial in the lubrication study of the nanoparticle and bovine calf serum. (Chicken) egg white was used for the experiment. The egg white was separated from the egg yolk and no further treatments were made.

3.2 Tribological and Surface Characterization Tools

3.2.1 Tribometer

A pin-on-disk tribometer (CSM Instruments) was used for carrying out the Tribology tests. As the name 'tribometer' suggests, 'tribos' meaning rubbing and 'meter' meaning measurement, is an instrument which is used to measure the friction and wear of different materials. Friction and wear is measured by moving the two material surfaces relative to each other. Various parameters like speed, frequency, normal load, contact pressure, time, humidity, lubricant, temperature, motion etc can be controlled to simulate the real life wear processes occurring in the industry. The first wear testing machine was developed by Mr Charles Hatchet[111]; the design was such that there was a continuous change of rubbing direction to avoid accelerated wear. But the modern tribometers have the pin running on the same wear path.

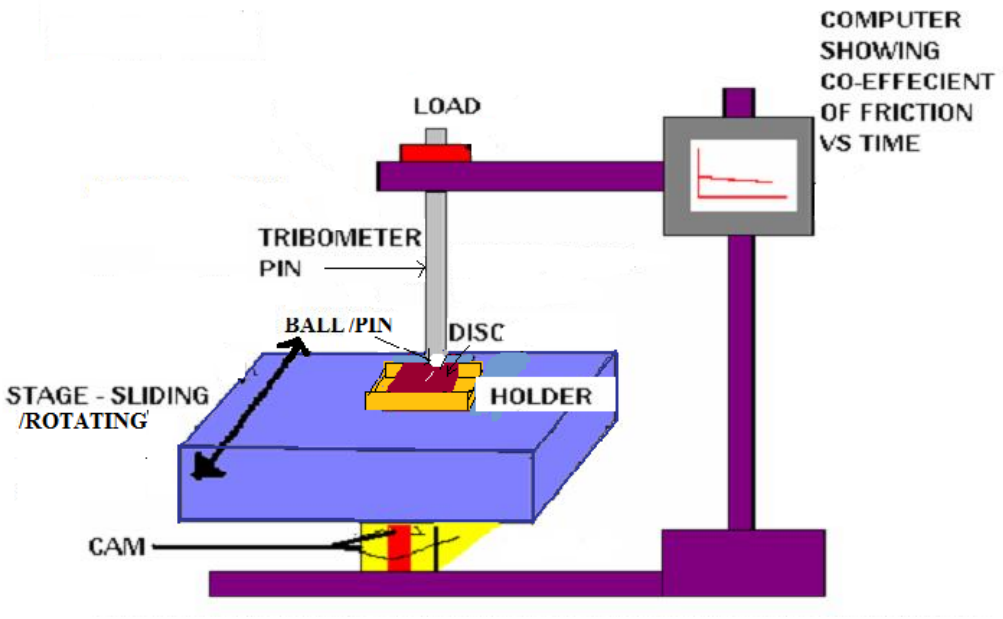

Figure 3.7. A pin-on-disk tribometer.

In this research, a pin–on-disk tribometer was used for the experiments. Since our focus was to study the friction and wear of the (alumina) coatings and to understand the basic elements in lubrication, such a test rig was sufficient to serve the purpose.

A pin-on-disk tribometer is shown in the figure 3.7. The pin could be spherical, pin or flat. The holder holds the disk and the disk could be of varying size and shape. The pin has a stable contact point with the disk. As shown in the figure, a pin/ball is moved over the sample by means of a stage which could either be rotating or reciprocating. Thus the tribometer can work for both reciprocating and rotating modes. The sample and the counter face sliding partner could be of different materials. The desired normal load is placed on the tribometer pin and the speed is applied via the stage. The tribometer arm measures the tangential force which is then transmitted to the controller through the sensors. The controller uses this data and presents the output on

the computer as a plot of co-efficient of friction vs. time. Wear data can be calculated by using the volume of material lost during the test. It could also give the plot of coefficient of friction against the distance and the number of cycles. The experiment can also be performed in a controlled environment i.e. different temperature, vacuum etc using specially designed chamber and special heating stage accessories.

A pin-on-disk tribometer (CSM Instruments) with the reciprocating stage was used to calculate the friction and simulate the wear for the Alumina coatings whereas for the lubrication study of the gold nanoparticles in serum, a rotating stage was used to simulate the joint movement.

3.2.2 Profilometer

A profilometer is a surface characterization technique which is used to study the topography of a sample surface. It is used to measure the surface profile in order to quantify its roughness in either microinches or micrometers. It measures its surface roughness by either contact mode or non-contact mode. The contact mode has a very sensitive stylus probe which is made of diamond like material. The lateral and vertical movement of the stylus across the sample generates an analog signal. This analog signal is then converted to digital signal which is stored, analyzed and displayed. It can also be used to measure the surface waviness. A typical surface Profilometer is shown in the figure 3.8.

Figure 3.8. The TR 200 portable surface profilometer.

The profilometer shown in the figure above is TR 200 hand-held surface tester. The TR200 measures surface roughness and the wear profile using a sharp stylus (or tip) attached to it. This tip is placed on the surface of the part and then traced at a constant rate. The roughness causes the change of inductive value of the induction coil which generates an analog signal which is proportional to surface roughness. This signal enters data collection system after amplification and level conversion. The profilometer measures various parameters, Ra, Rz, Ry, Rq, Rp, Rm and so on. Table 3.4 shows the various surface roughness parameters that can be obtained using the profilometer[112].

As the reading parameter, we choose the "Ra", commonly defined as the arithmetic mean of the absolute values of profile deviation form mean within sampling length.

Table 3.4
Major surface roughness parameters obtained using the TR 200 surface profilometer

Parameter	***Name***
Ra	Roughness Average (Ra)
Rq	Root Mean Square (RMS) Roughness
Rt	Maximum Height of the Profile
Rv, Rm	Maximum Profile Valley Depth
Rp	Maximum Profile Peak Height
Rpm	Average Maximum Profile Peak Height
Rz	Average Maximum Height of the Profile
Rmax	Maximum Roughness Depth
Rc	Mean Height of Profile Irregularities
Rz(iso)	Roughness Height
Ry	Maximum Height of the Profile

Along with the surface roughness it can also be used to study the topography. The topography can be used to obtain a 2D image of the peaks and valleys of the surface and the wear track. Thus it can be used to compare the change in the surface after the tribology test. The wear profile will give us the width and the depth of the wear track, whereby we can calculate the wear area which can then be used to calculate the wear volume and also the volumetric wear rate.

3.2.3 SEM (scanning electron microscope)

A scanning electron microscope is one of the most powerful and widely used tool for surface characterization. It is a type of electron microscope that scans the surface with a beam of electrons in a raster scan pattern.

HISTORY: The idea of using charged particle beam was first proposed by Stintzing in 1929 in Germany[113]. But it received its much popularity when the first scanned electron image was produced by Max Knoll in 1935. He imaged silicon steel showing electron channeling contrast[114]. Further pioneering work was performed by Professor Sir Charles Oatley who invented the SEM in its current form[115]. It was first made commercial in 1965 by the Cambridge International Company as the 'Stereoscan'. Their first client was DuPont.

WORKING: An electron beam is produced by a gun and accelerated by the high voltage created between the wire and the node. This beam is focused by the electromagnetic lenses on the sample. These electrons interact with the surface atoms and provide signals informing about the surface's morphology, elemental composition, topography and other properties. The type of signals include secondary electrons, back scattered electrons, light, characteristic X-rays etc. These signals are gathered by the detector which then converts it into an electric signal. All of these signals can be used to interpret different type of information about the surface. Secondary electrons can be used to produce very high resolution images of the sample surface. The X-rays are used to study the elemental composition of the sample and the back-scattered electrons can be used both for imaging and for the elemental analysis.

Figure 3.9. A JEOL JSM 6400 scanning electron microscope.

ADVANTAGES AND DISADVANTAGES: The advantages of SEM are that it has a higher resolution than the optical microscope and is faster than the scanning probe microscopes. It can be used to provide both the images and the elemental composition of any surface. But the disadvantages are that it requires a conductive sample and that all the imaging must be carried out in vacuum etc.

JEOL JSM 6400 Scanning Electron Microscope (SEM) was used for the wear analysis of the MAO alumina coatings. The SEM used is shown in the figure 3.9.

3.2.4 TEM (transmission electron microscope)

Transmission Electron microscope is a microscopy technique in which a beam of electrons is used to image the object in the order of a few angstroms. The TEM can be used to determine:

1. Morphology: size, shape and arrangement of the particles on the surface
2. Crystallographic information: arrangement of atoms and their order, atomic scale defects
3. Compositional information: composition of elements and compounds and their relative ratios.

Thus TEM is an important tool for medical, biological and material research.

HISTORY: The first transmission electron microscope was built in 1938 using concepts of Max Knoll and Ernst Ruska[116] by Albert Prebus and James Hillier at the university of Toronto. The principle is that when a beam of electrons pass through an ultra thin specimen, an image is formed which can be magnified and focused by an objective lens and which appears on an imaging screen.

WORKING: An electron source emits electrons which pass through a vacuum column of the microscope. It uses electromagnetic lenses to focus the electrons into a thin electron beam. This electron beam then passes through the specimen. Some of the electrons get scattered while some get dispersed while the unscattered electrons hit a fluorescent screen which gives rise to an image with different parts displayed in varied darkness depending upon their density. The sample preparation for imaging in TEM is very tedious and time consuming, but the resolution is very high. Typical resolution of the

modern TEM is < 2 Å. The best resolution achieved so far is 0.6 Å. It can be used for imaging, chemical and elemental characterization[117].

ADVANTAGES AND DISADVANTAGES: The advantages of using a TEM are its very high resolution in the order of angstroms. It can also be used to study the internal structure. The disadvantage is the long time required to prepare a sample.

A JEOL JEM 6400 Transmission Electron Microscope was used to study the surface morphology of the before and the after tribology test of different concentrations of nanoparticles. The TEM used for the experiment is shown in the figure 3.10.

Figure 3.10. The JEOL JEM-2010 transmission electron microscope.

3.2.5 Rheometer

It is used to measure the way in which a liquid, suspension or slurry flows in response to applied force. It measures the viscoelastic properties: yield stress, modulus, creep, complex viscosity, kinetic property etc. It can be used in pharamaceutical, foods, cosmetics, pavement, medical, biological fields etc. They are of two types:

1. Shear rheometers
2. Extensional rheometers

HISTORY: The word 'rheometer' comes from the Greek word 'rheo' meaning flow, thus it is the device used for measuring the flow. Earlier in the 19th century it was used to measure electric current before the words galvanometer and ammeter were discovered.

WORKING: It is a mechanical spectrometer which subjects a sample to either a dynamic or a steady shear strain and then the transducer measures the resultant torque. The other properties can then be calculated using the torque data.

The viscosity was measured using an AR-G2 Rheometer, TA instruments. Figure 3.11 shows the Rheometer used. It is the only Rheometer which offers unique separate motor and transducer technology and thus measures stress independently of the shear deformation[118]. The viscosity and shear stress were measured for the different concentrations of nanoparticles: 0%, 25%, 50% and 75% and at different velocity.

Figure 3.11. Ar-G2 rheometer. (TA instruments)

3.3 Tribology Test Conditions

3.3.1 Friction and wear study of the alumina coatings

A pin-on-disk tribometer (CSM Instruments) was used for carrying out the friction and wear tests. The experimental setup is shown in Figure 3.12. The disks were the alumina coatings on the aluminium substrate while the pin was a silicon nitride ball of 6 mm diameter. The disks were submerged in the SBF for the entire time during the tests to simulate the biological environment.

The ball was rigidly fixed in the tribometer pin and the disks were reciprocated at a linear speed of 2.5 cm/s. The length of the wear scar or the amplitude was selected as 6 mm. The tests were carried out at a normal load of 5 N for 8 hours (28800s) at 25° C.

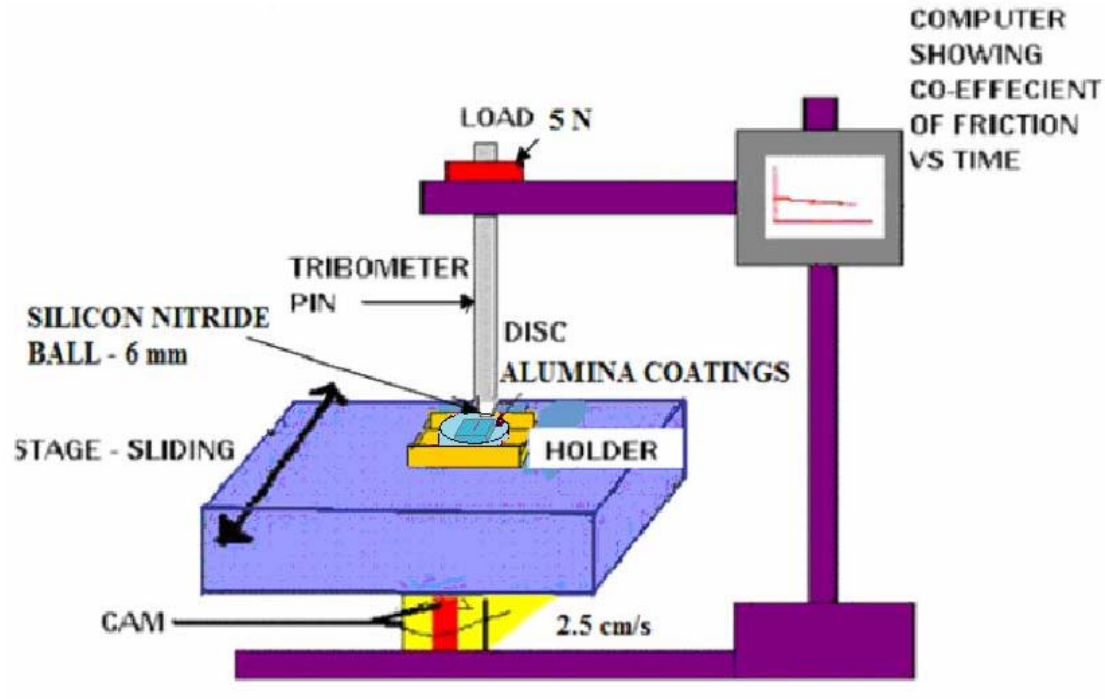

Figure 3.12. Experimental setup used to test the MAO alumina coatings.

Thus the wear was simulated using a pin-on-disk Tribometer and the surface was characterized using a TR 200 stylus profilometer and a JEOL JSM 6400 SEM (Scanning Electron Microscope). The stylus profilometer was used to measure the surface roughness and to study the profile of the wear track. The scan distance for the stylus was set at 4 mm and the roughness range was set between ±80 microns. The SEM was used for imaging the wear track to study their surface morphology.

3.3.2 Lubrication study of the nanoparticles

To study the effect of nanoparticles on lubrication the Stribeck curve was plotted; the Y-axis of the Stribeck plot was the coefficient of friction whereas the X-axis was the Sommerfield number. The Sommerfield number is viscosity x velocity/load.

VELOCITY: Four different speeds were selected: 1.25 cm/s, 2.5 cm/s, 3.75 cm/s and 5 cm/s. The speeds were selected in accordance with the age and the activity. For the very old people 1.25 cm/s was selected, 2.5 cm/s was for standard walking whereas 3.75 cm/s and 5 cm/s were for jogging and running respectively.

LOAD: Three different loads: 1N, 3N and 5N were chosen based on the weight of the person and the amount of force acting on the joint.

The Sommerfield numbers were calculated for the different concentrations (25%, 50% and 75%) and different velocities (1.25 cm/s, 2.5 cm/s, 3.75 cm/s and 5 cm/s) and different loads (1N, 3N and 5N).

The coefficient of friction was obtained using the Tribometer for different loads and speeds. A rotating slide was chosen to simulate the natural joints. The pin was a stainless steel ball having a diameter of 6 mm and the disk was a glass slide. Serum and the nanoparticles (depending upon the concentration) were mixed for 5 minutes and then placed on the glass slide which was on the rotating stage. Each test was run for 1 minute by which time the friction had stabilized. The experimental setup used is shown in figure 3.13.

The viscosity was calculated for different load and different velocity at different concentration using a Rheometer. These values were then used to calculate the Sommerfield number and plotted against the co-efficient of friction to obtain the Stribeck plot.

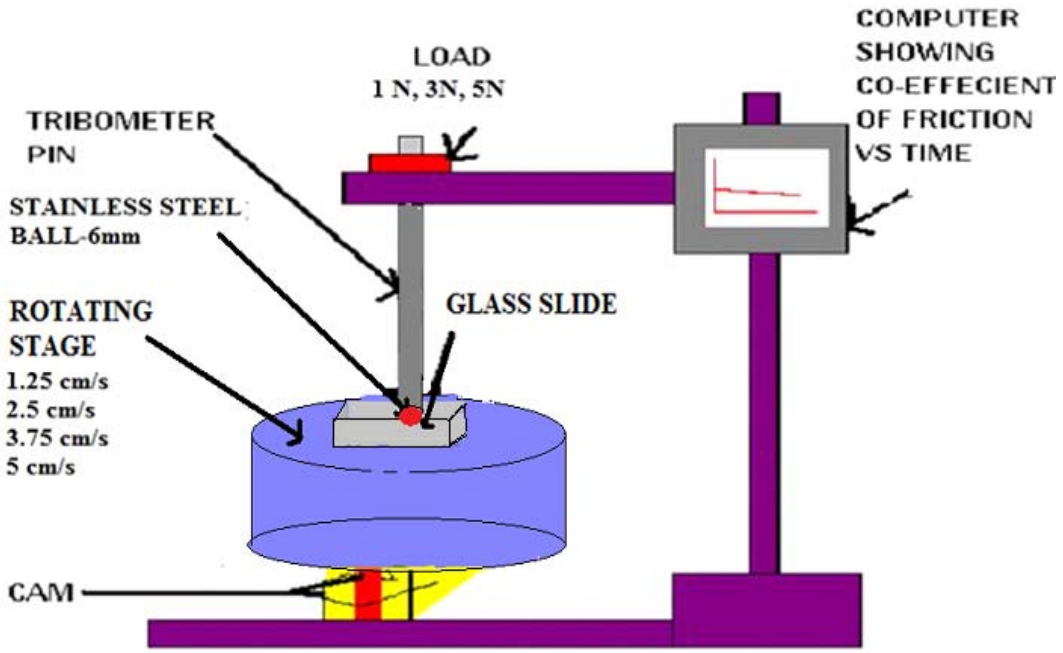

Figure 3.13. Experimental setup used for the lubrication study.

4. TRIBOLOGICAL CHARACTERIZATION OF ALUMINA COATINGS

As mentioned in section 1, ceramic-on-ceramic joints have the least friction and show the lowest wear among all the other bearing pairs. Further study of alternative ceramic coatings could lead to better understanding of such materials. In this research, silicon nitride on MAO alumina coatings was tested to characterize the alumina coating for artificial joints. In order to understand the tribological behavior of the MAO alumina coatings in biological environment, pin-on-disk tribometer was used to create wear and study the friction, profilometer was used to study the profile of the wear and SEM was used to study the morphology of the wear track and the weartrack-surface interface. This section discusses tribological properties of MAO alumina coatings.

4.1 Frictional Behavior

Friction was measured using a pin-on-disk tribometer and the coefficient of friction was measured while the tests were being conducted and mapped against time. The tests were run for 8hrs or 38198 cycles at 2.5 cm/s with a 5N load. The coefficient of friction vs. time for all the three coatings is shown below.

Figure 4.1 shows the coefficient of friction vs. time plot for 0.100 A/cm^2 coating. The friction started high at 0.349, reaching a maximum of 0.371 and then decreased and remained constant at a mean value of 0.192 with a std. deviation of 0.029.

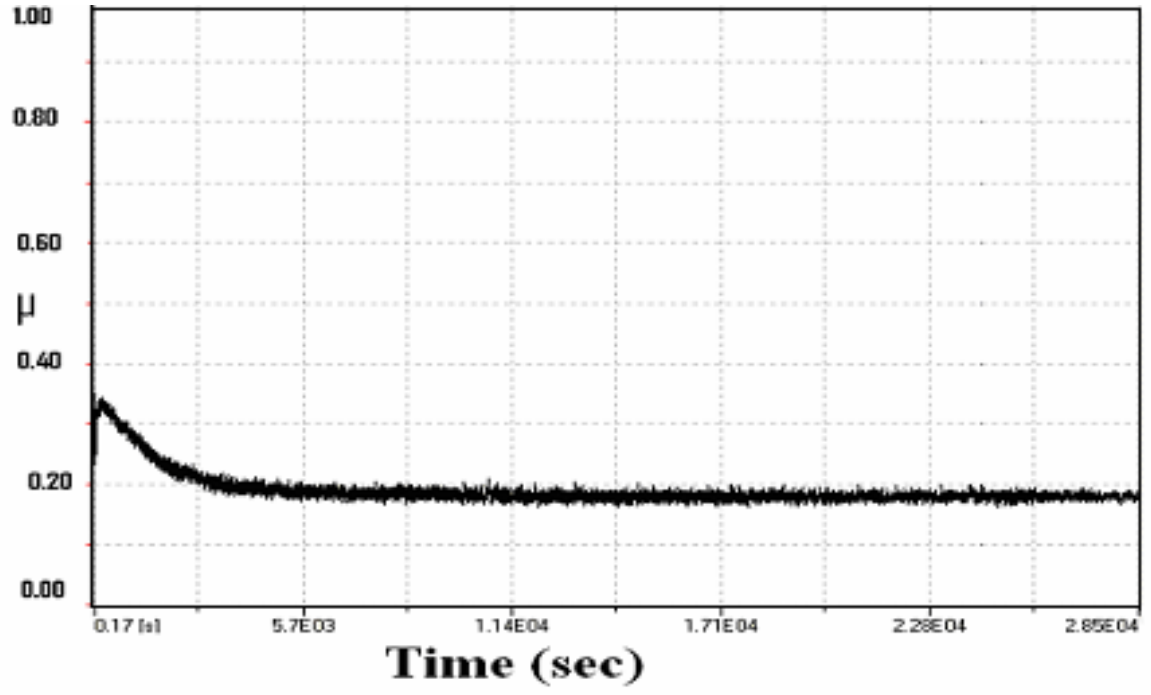

Figure 4.1. Coefficient of friction vs. time for the 0.100 A/cm^2 coating.

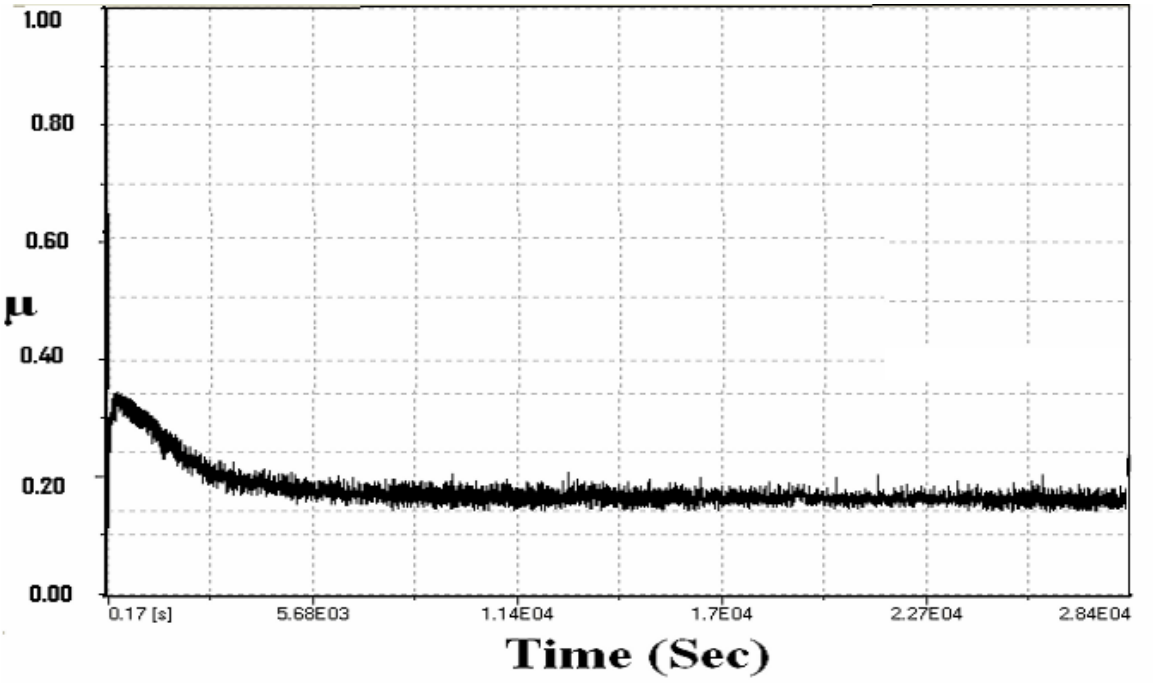

Figure 4.2. Coefficient of friction vs. time for the 0.125 A/cm^2 coating.

Figure 4.2 shows the coefficient of friction vs. time plot for 0.125 A/cm^2 coating, the maximum friction was 0.246 which then decreased and remained steady at a mean value of 0.175 and a standard deviation of 0.019.

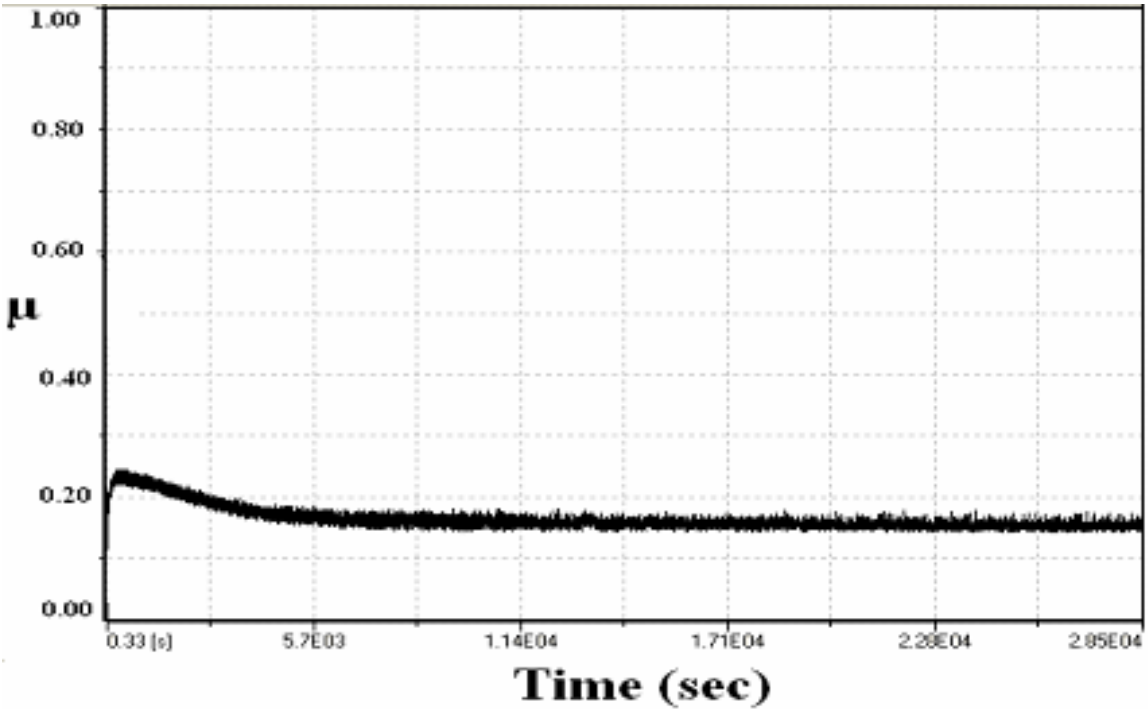

Figure 4.3. Coefficient of friction vs. time for the 0.150 A/cm^2 coating.

Figure 4.3 shows the coefficient of friction vs. time plot for 0.150 A/cm^2 coating, the maximum friction was 0.243 and the constant mean value was 0.167 with a standard deviation of 0.018.

For all the three coatings, the coefficient of friction started high, then decreased and then remained constant with time. The initial increase is due to 'running in' period where the surface roughness played a major role. After the initial 'running in' period as

can be seen from the plots, the friction coefficient became stable and remained consistent throughout the entire test.

Table 4.1 shows the starting, minimum, maximum, mean and standard deviation of the coefficient of friction obtained for all the three MAO coatings. As can be seen from the table, the mean coefficient of friction is least for the 0.150 A/cm^2 coating followed by 0.125 A/cm^2 and finally the 0.100 A/cm^2 coating.

Table 4.1
Summary of the friction coefficients for the MAO coatings

Sample	***Start***	***Min***	***Max***	***Mean***	***StdDev***
0.100 A/cm^2	0.349	0.158	0.371	0.192	0.029
0.125 A/cm^2	0.189	0.067	0.246	0.175	0.019
0.150 A/cm^2	0.332	0.117	0.243	0.167	0.018

The 0.150 A/cm^2 coating produced the lowest mean friction while the 0.100 A/cm^2 coating produced the highest mean friction. This might be due to two reasons: One is the low shear force involved during sliding resulting from a hard surface being cut by a soft one. The other is the formation of a solid lubricant due to introduction of wear debris.

Difference in the friction is also because of the phases present in the coatings. Since these coatings were produced using an ac power supply, mixed α-Al_2O_3 and γ-Al_2O_3 phases were produced which resulted in higher hardness, higher density and

elevated corrosion resistance[119]. Also, the increase in the time and the current intensity, increases the amount of α-Al_2O_3[120]. Due to the difference in the current intensities, there is a difference in the amount of α-Al_2O_3 and γ-Al_2O_3 produced. Therefore the 0.150 A/cm^2 coating which has both the α-Al_2O_3 and γ-Al_2O_3 phase is much harder and more corrosion resistant than the 0.125 A/cm^2 coating which has only the γ-Al_2O_3 phase which is harder than 0.100 A/cm^2 sample which has neither of the phases. This corresponds with the results obtained using the scratch test shown in table 3.1. Since the 0.150 A/cm^2 is the hardest it gives a lower coefficient of friction as compared to the other two coatings. This indicates that a hard-and-soft rubbing pair generates a low friction with a low shear stress during sliding.

4.2 Wear Mechanisms

A scanning electron microscope was used for imaging the wear track-surface interface and for comparing the surface and the weartrack morphology. Figures 4.4, 4.5 and 4.6 show the wear track-surface interface at 200 microns or 150 X magnification, with the white line showing the demarcation between the two regions while the figures 4.7, 4.8 and 4.9 compare the wear track and the surface at a greater magnification at 16 microns or 2000 X magnification.

The as-received surfaces were extremely rough as will be evident from the figures below. The reason for the rough surface was that during the Micro Arc Oxidation (MAO) process, the thickness of the coating is controlled by the molten alumina which flows out of the discharge channels. This alumina cools down rapidly forming a sharp

and visible boundary leaving behind a disc-shaped structure. As the thickness keeps on increasing, the layers keep on forming over each other, thereby covering these disc structures. But during the last stage of the MAO treatment, some of these discharge channels remained open while some get closed and are visible on the surface.

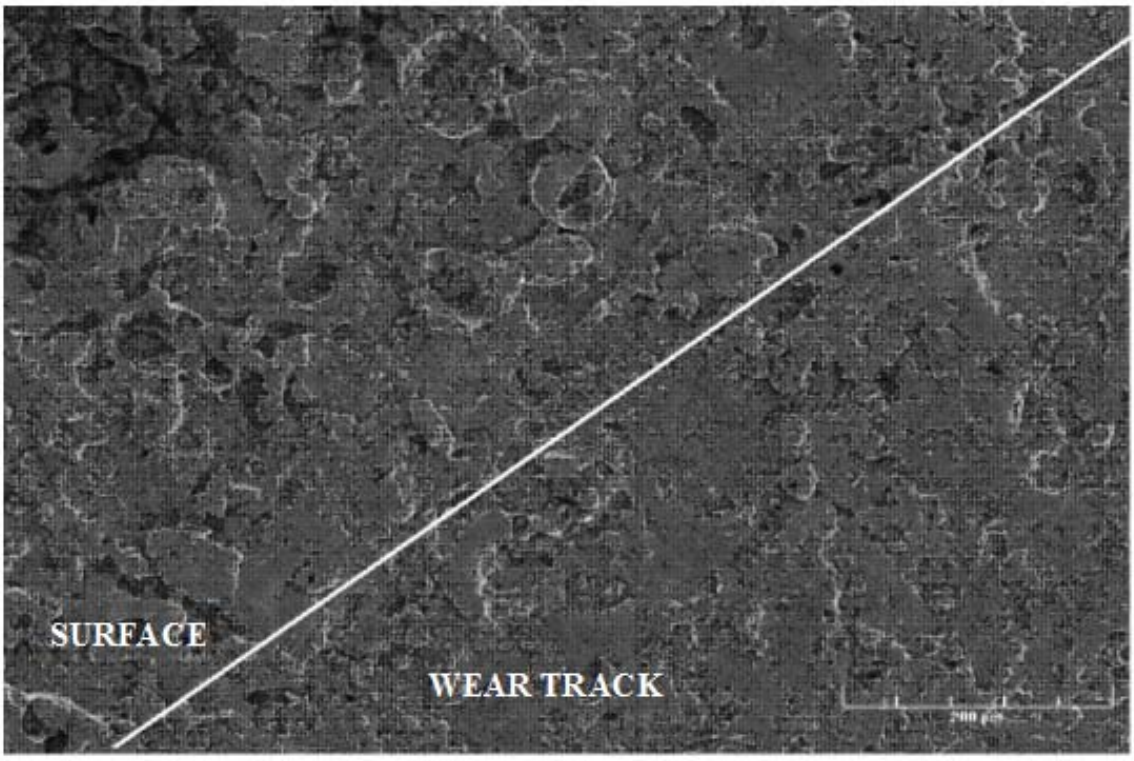

Figure 4.4. Weartrack-surface interface of 0.100 A/cm^2 coating.

Figure 4.4 shows the disc shaped structures on the as-received surfaces, they are wide and some of them are closed while some are open whereas the wear-track is much smoother. The disc structures have flattened out and merged into each other forming a flat and smoother surface.

The same type of flattening was observed in figure 4.5. Both of these images show that somehow even after 8 hours of testing, the wear track was smoother and flatter than the original as-received surface.

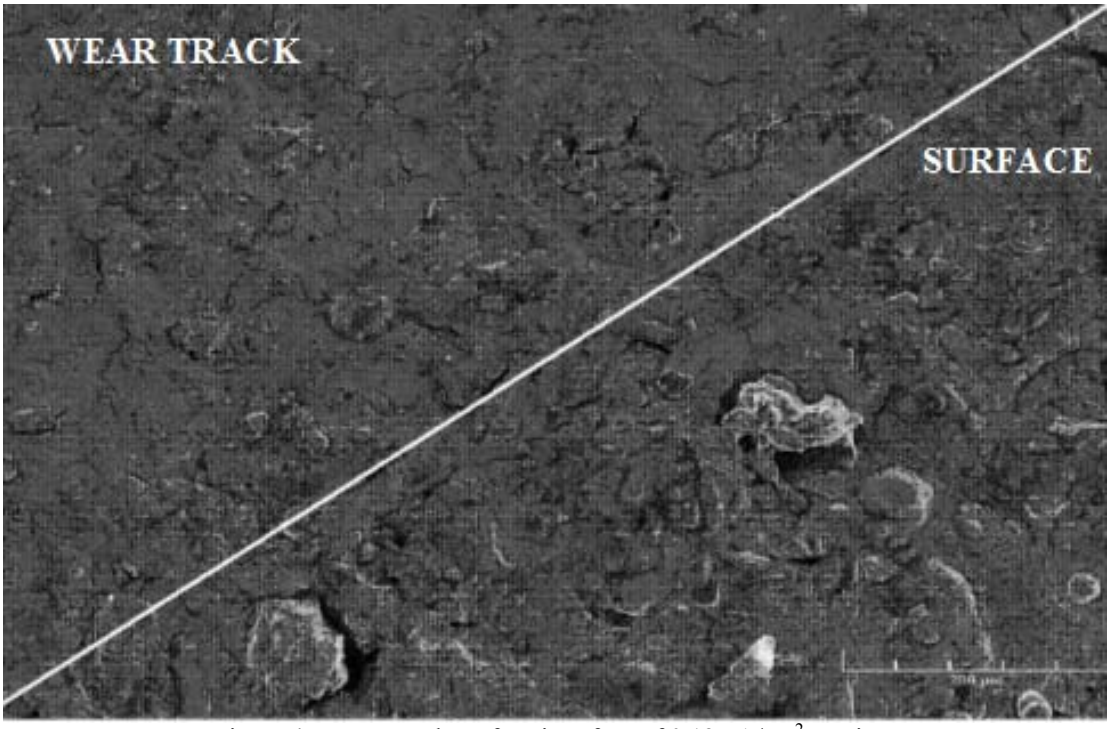

Figure 4.5. Weartrack-surface interface of 0.125 A/cm^2 coating.

For the 0.150 A/cm^2 coating seen in the Figure 4.6, the disc structures on the as-received surface are more in number and smaller in size. This is because of the difference in the current intensities. With an increase in the current intensity, the amount of molten Alumina flowing out is more, leading to more number of discharge channels. Also if we observe the three coatings, the blank spaces between the discharge channels were more in the 0.100 A/cm^2 coating as compared to the 0.150 A/cm^2 coating. Thus due

to more number of discharge channels and less space between these discharge channels, the 0.150 A/cm^2 coating is more uniform and stable.

Figure 4.6. Weartrack-surface interface of 0.150 A/cm^2 coating.

To study the wear mechanism, the three coatings were observed at a much higher magnification using the SEM.

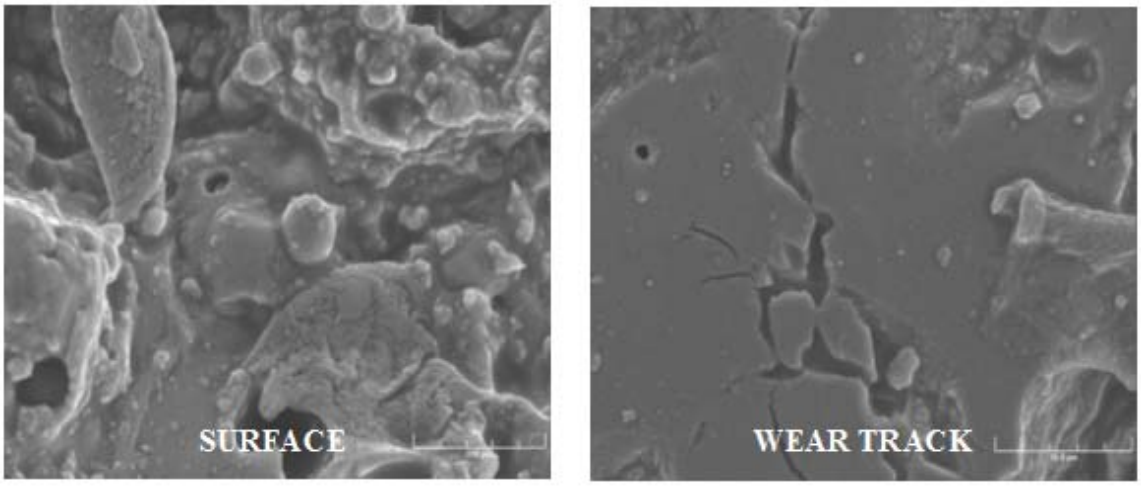

(a) (b)

Figure 4.7. (a) Surface and (b) Weartrack for 0.100 A/cm^2 coating.

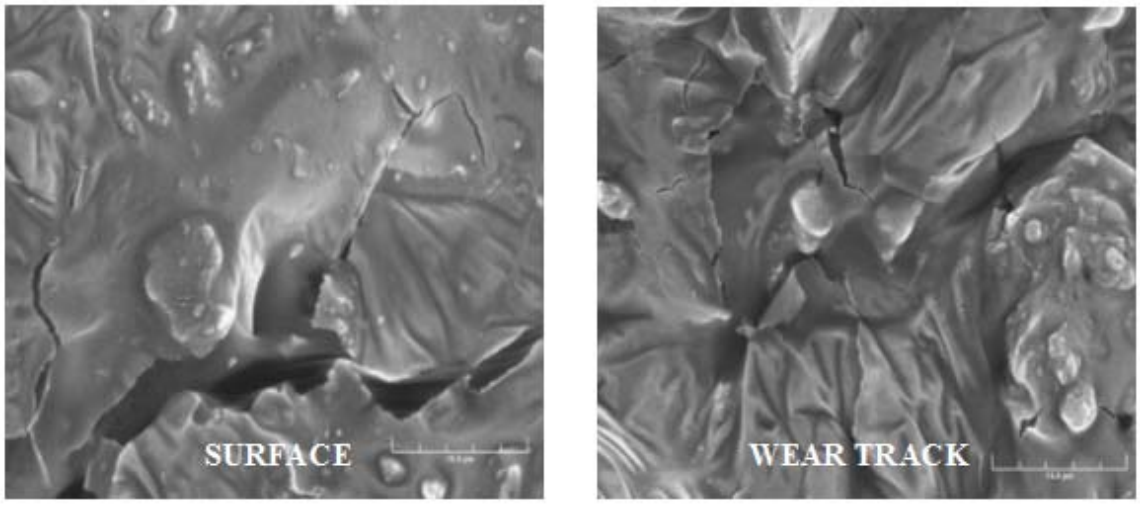

(a) (b)

Figure 4.8. (a) Surface and (b) Weartrack for 0.125 A/cm^2 coating.

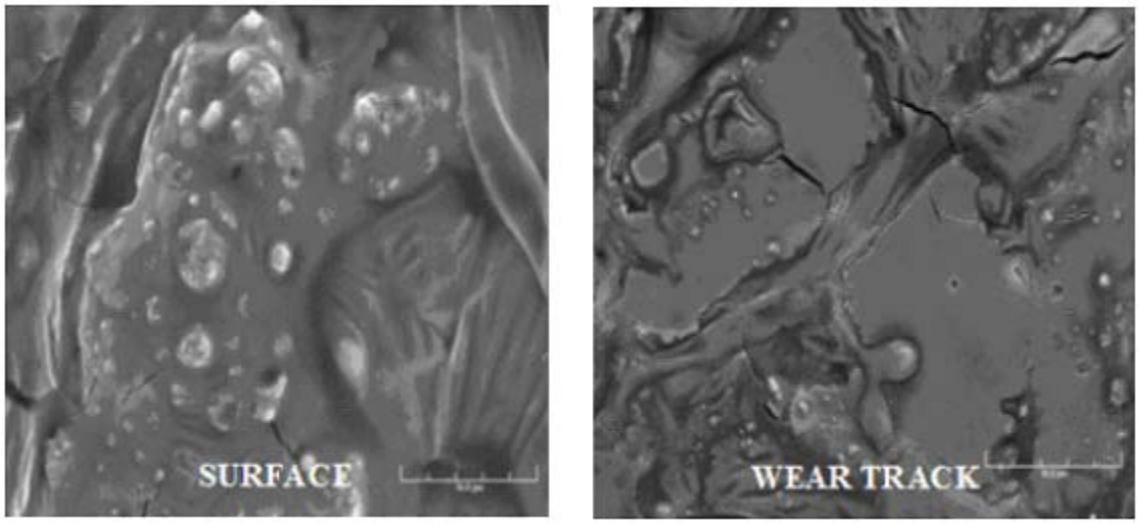

(a) (b)

Figure 4.9. (a) Surface and (b) Weartrack for 0.150 A/cm^2 coating.

The images at higher magnification show the as-received surfaces to be very rough and the wear track to be very smooth. The surface of the weartrack was also more flat. It is because of the ploughing effect wherein the disc structures had more or less flattened out and merged into each other, leaving cracks in some places but the coating still adhered to the substrate. Cracks are observed on the wear track, which indicates that the wear mechanism was abrasion with micro fracture.

Also no significant tribochemical reactions[122] were seen on the wear track on using the SBF. This indicates the stability of the MAO coating in the SBF environment.

4.3 Wear Profile

Along with the images obtained using the SEM, the wear tracks were also studied using a TR 200 Stylus profilometer. The stylus was scanned for a distance of 4 mm and a surface roughness range of ±80 μm. The profilometer was scanned in the

direction perpendicular to the wear track and the profiles are obtained. Figures 4.10-4.12 show the wear profiles for the three coatings. The curve in the profile illustrates the depth and the width of the wear track.

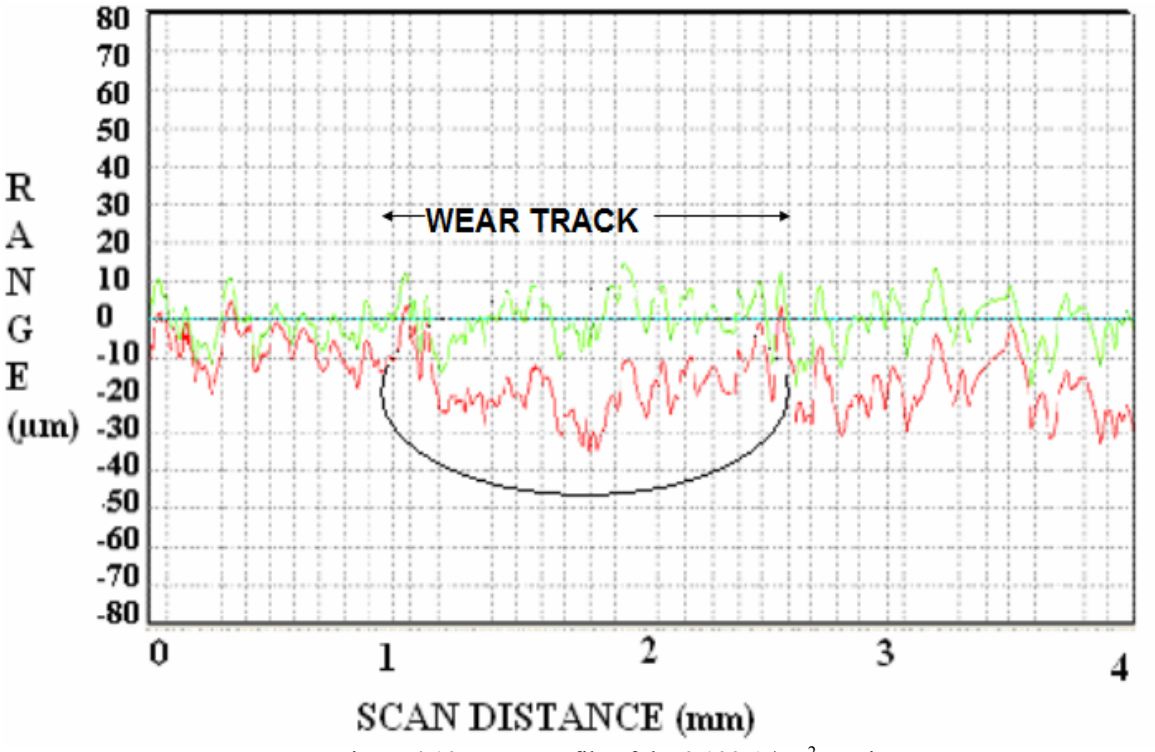

Figure 4.10. Wear profile of the 0.100 A/cm^2 coating.

The green curve is the filtered profile which shows the wear with respect to the zero axes whereas the red curve is the original profile of the wear track. The wear-track of each coating is indicated on the graph.

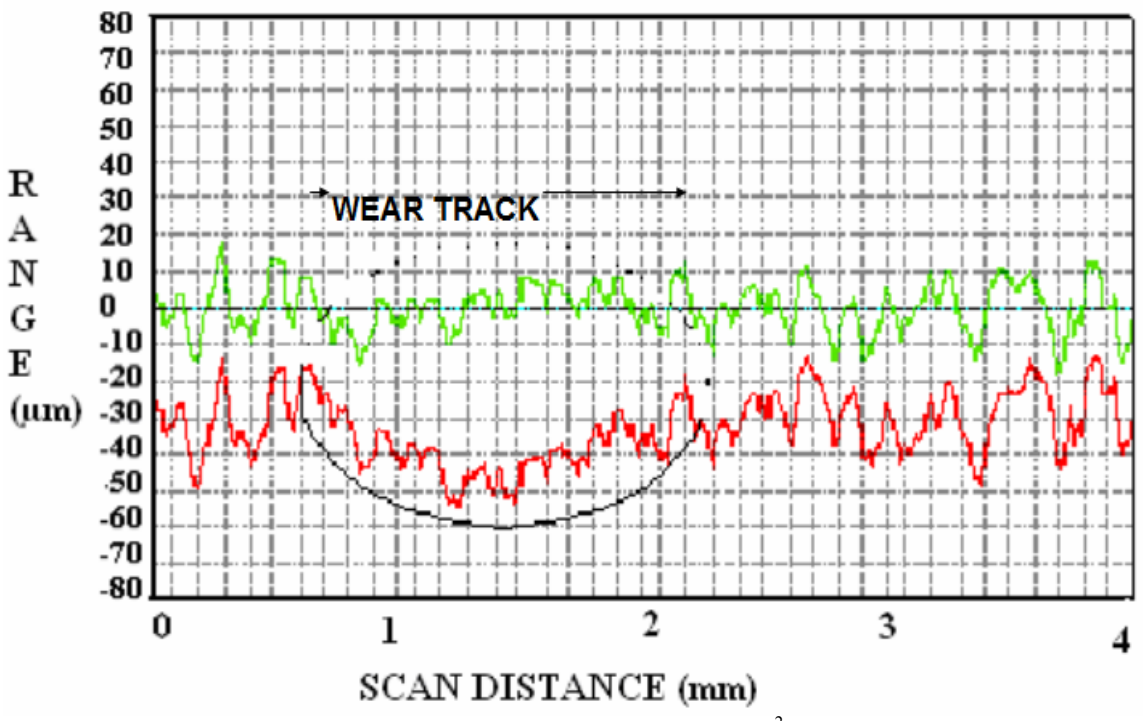

Figure 4.11. The wear profile of the 0.125 A/cm^2 coating.

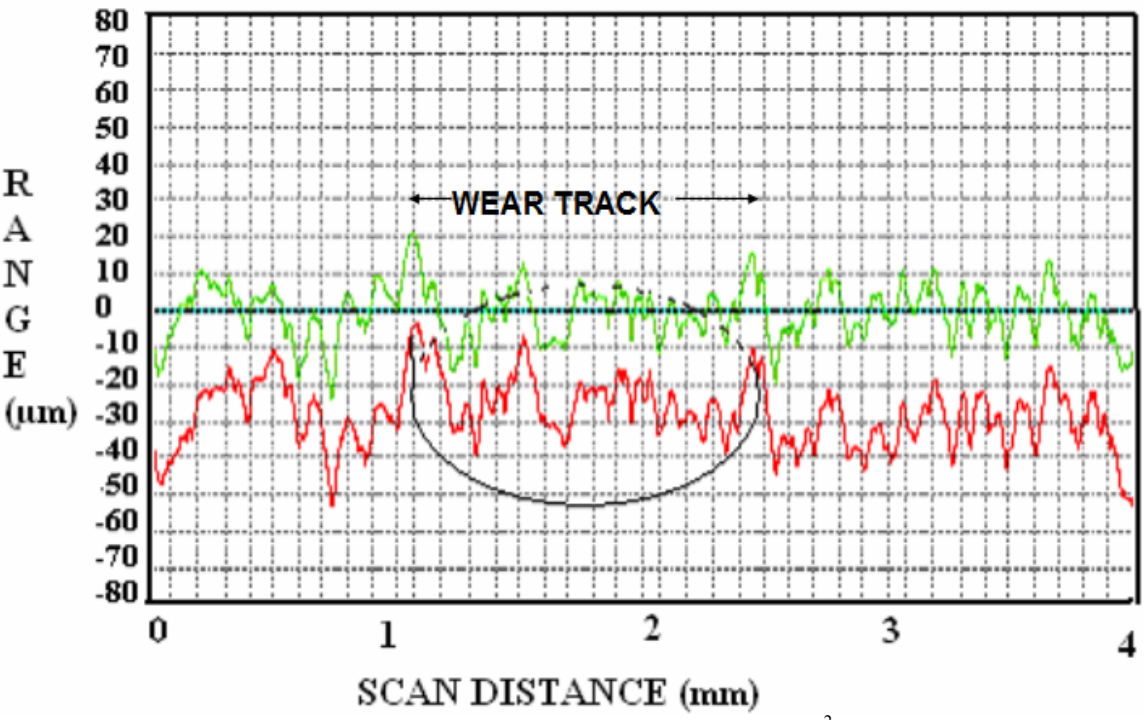

Figure 4.12. The wear profile of the 0.150 A/cm^2 coating.

As can be seen from the wear profiles above, there is not much change in the profile between the wear track and the as-received surface of the coating, which indicates that inspite of the wear test being carried out for 8 hours using silicon nitride, the resultant wear profile has not shown much change as compared to the surface. There is only redistribution of mass in the wear track and SBF has also acted as a lubricant making the surface smoother.

4.4 Wear Scar on the Ball

Due to sliding between the coatings and the silicon nitride ball a corresponding wear was found on the ball. The SEM images of the wear scars were taken and the wear scar diameters measured and are listed in Table 4.2**.** As can be seen from the Table 4.2, the wear scar diameter is highest for the ball against the 0.100 A/cm^2 coating, while it is lowest for the 0.150 A/cm^2 coating. It was interesting that the friction found on this pair was the lowest.

Table 4.2
Wear scar diameter on the ball

Coating	***Wear Scar Diameter (mm)***
0.100 A/cm^2	1.267
0.125 A/cm^2	1.217
0.150 A/cm^2	1.111

The underlying reason is because of the γ Al_2O_3 and α Al_2O_3 phases present in the 0.150 A/cm^2 coating, which makes the 0.150 A/cm^2 coating very stable. Thus there is a low wear on the ball and low co-efficient of friction.

4.5 Remarks

The results obtained from the frictional data, the surface morphology, the wear profile and the wear scar on the ball, indicates that the coatings are highly wear resistant in the Synthetic Biofluid environment.

The tribological investigation on MAO coatings in SBF were carried out and the effects on microstructure, friction and wear were studied. The friction was measured using a tribometer, and SEM and profilometer were used to characterize wear. Both of these data indicated the stability of the alumina coatings in the SBF environment. The friction obtained was least for the 0.150 A/cm^2 coating which also showed less corresponding wear scar diameter on the ball. On studying the morphology and profile of wear tracks, it was concluded that there was only redistribution of mass on the coating and the wear mechanism was found to be abrasive with microfracture.

5. EFFECTS OF NANOPARTICLES ON FLUID LUBRICATION

To study the effects of nanoparticles on lubrication, a "Stribeck" curve of biofluid was generated for the different concentration of spherical and rod-shaped nanoparticles. The changes in the surface morphology, before and after tribology tests were characterized in order to evaluate effects of nanoparticles on lubrication. The objective of this part of research is to obtain basic understanding of fluid lubrication and to open new areas of investigation in nanomaterial and lubrication areas.

5.1 Rheology Results

The various properties of fluid such as viscosity, shear stress and shear rate were studied using the AR G2 Rheometer. According to the Newton's law of fluid friction, the fluid between any two surfaces in relative motion with each other can be divided into many parallel layers such that each layer will be moving at its own velocity[123]. This gives rise to two very important rheological properties: viscosity and shear stress. Viscosity is defined as the 'resistance to flow' or it is the internal molecular friction which exists between the two layers rubbing against each other. Thus a low viscosity fluid flows easily as compared to a high viscosity fluid. For any fluid, shear stress is the force that is required to move one layer past the other. For the pin-on-disk tribometer, silicon nitride ball was held stationary in the pin and the glass slide was rotated. The biofluid in between these two surfaces could be divided into many parallel layers as shown in the figure 5.1. Keeping the shear rate constant, viscosity and shear stress were

measured for different concentration of spherical nanoparticles in serum. Figure 5.2 shows shear stress vs. shear rate while figure 5.3 shows viscosity vs. shear rate for all the four concentrations.

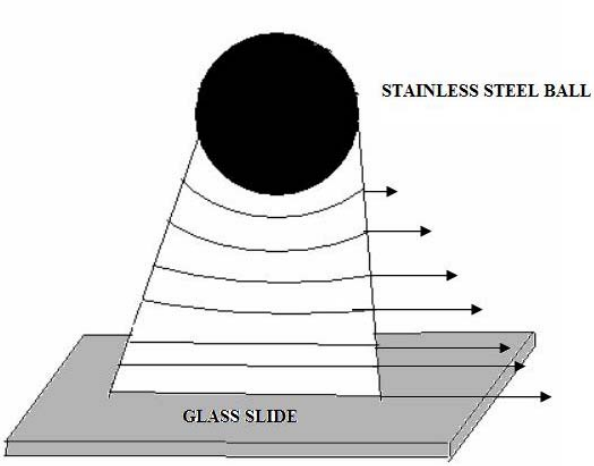

Figure 5.1. The different layers between the stainless steel ball and the glass slide.

Figure 5.2 shows the shear stress vs. shear rate for all four concentrations. With the addition of nanoparticles, the shear stress has increased correspondingly. The 75% fluid shows the maximum shear stress whereas 0% shows the minimum. It shows that with the addition of nanoparticles, the force required to displace one layer against the other has increased which is why the shear stress has also increased. There are two interactions in the fluid; one is the interaction between the nanoparticles and the protein; and the other is between protein and protein. The shear stress shows an increasing trend with shear rate till 50 s^{-1}. At the shear rate of 50 s^{-1}, the shear stress is maximum and then the shear stress decreases with the shear rate. Thus, 50 s^{-1} can be considered as the critical shear stress. After the critical shear stress, the interactions between the

nanoparticle and the protein become dominant which is the reason for the decrease of the shear stress.

Figure 5.3 shows the viscosity to be minimum for the 75% concentration and maximum for the 25% concentration. Serum is a non-Newtonian fluid[124], i.e. the viscosity is not constant and changes with the shear rate. The solutions at 0%, 25% and 50% concentration show shear thinning behavior, i.e. their viscosity is decreasing with the increase in the shear rate. Whereas 75% concentration does not show any change with the shear rate.

The solution of 75% concentration shows maximum shear stress but minimum viscosity which suggests that the nanoparticles act as ball bearings providing little resistance to flow and thus showing minimum viscosity but due to the interaction between the proteins and the nanoparticles the shear stress is high. The 0% concentration has no nanoparticles showing minimum shear stress and a high viscosity due to protein-protein interaction. For 25% and 50% concentrations with the increase in the addition of the nanoparticles, the shear stress has increased; protein-nanoparticle interaction is the primary reason for such behavior. Also 25% concentration shows a higher viscosity as compared to the 50% concentration indicating that when more nanoparticles are added then the resistance to flow or internal molecular friction decreases, which decreases the viscosity but increases the shear stress.

To summarize, there are two competing mechanisms in the rheological behavior, the fluid flow and the interactions of fluid molecules and nanoparticles.

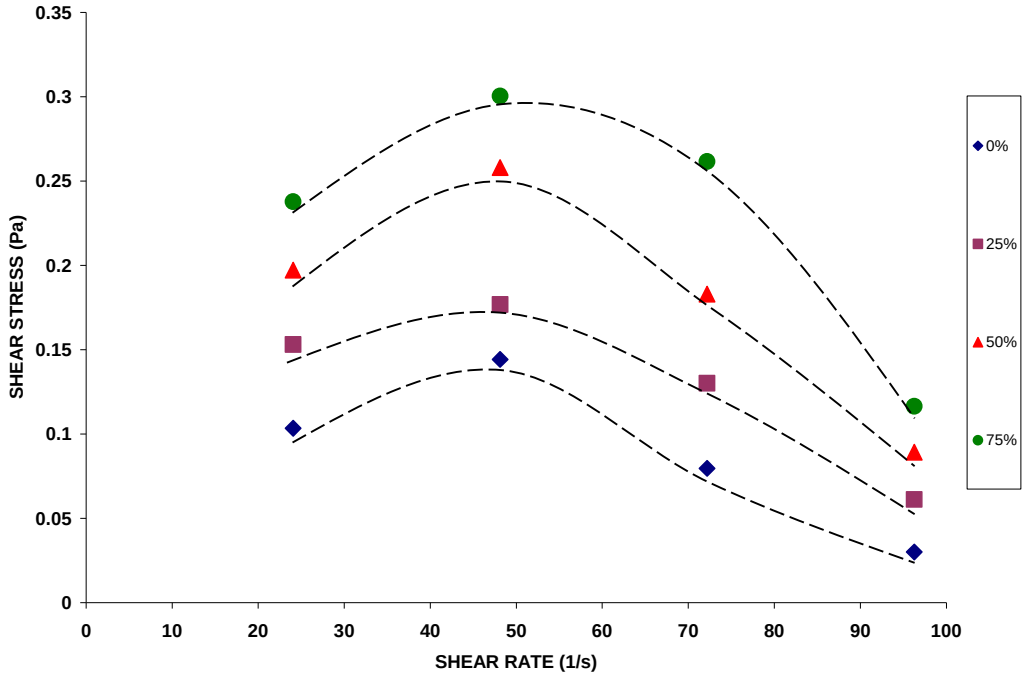

Figure 5.2. Shear stress vs. shear rate for all the concentrations.

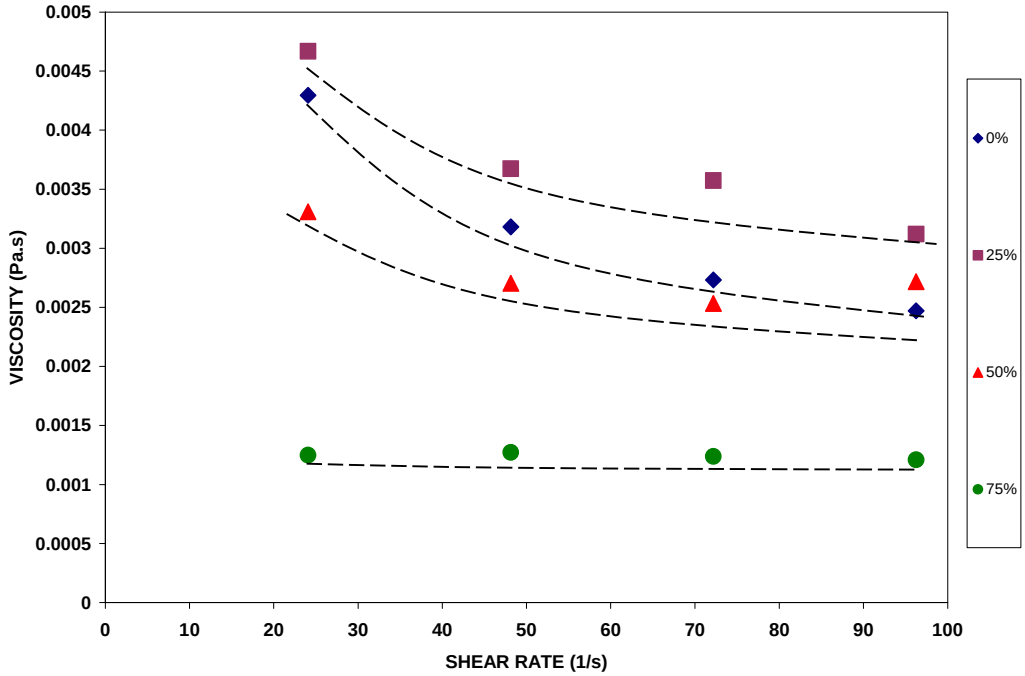

Figure 5.3. Viscosity vs. shear rate for all the concentrations.

5.2 Generation of a "Stribeck" Curve

5.2.1 Spherical nanoparticles

To study the lubrication effect of spherical nanoparticles in serum at different concentrations, a "Stribeck curve" was generated against the Sommerfield number. The viscosities at different velocities, loads and concentrations were measured with the rheometer. The friction force was measured as a function of velocity and load. The friction coefficient was then plotted against the Sommerfield number, as shown in the following figures. Figures 5.3, 5.4, 5.5 and 5.6 show the resulting Stribeck curves for the solution with 0%, 25%, 50% and 75% concentration of nanoparticles respectively. It has been reported in literature that the downward trend in the Stribeck plot indicates mixed lubrication regime whereas full film lubrication is indicated by an upward trend.

For all the Stribeck plots shown below, two distinct cases can be observed. One is for the lower load of 1 N while the other is for the higher loads of 3N and 5N. This difference in the behavior is because at higher load, a greater pressure is exerted by the stainless steel ball on the glass slide and hence the bio-fluid and the nanoparticle solution in between these two surfaces become thin. Because of this thinning of the solution, the viscosity of the solution plays an important role and the effect of nanoparticles becomes dominant which is seen in the form of lower coefficient of friction as compared to the lower load whereas at lower load, the interaction between the nanoparticle and the protein become dominant. This is consistent with the observation of rheological properties in previous section.

Figure 5.4 shows the Stribeck curve for the solution with no nanoparticles i.e. pure serum. The trends are decreasing for both higher and lower load, thus indicating mixed lubrication behavior, i.e., the load is carried partly by the surface asperities and partly by the lubricant. The coefficient of friction decreases since load is shared by both and there is less solid-to-solid contact. It has been proven that the proteins easily get adsorbed on the surfaces of materials[125] and the friction is affected by the number and the amount of proteins adsorbed on the surface. Thus mixed lubrication behavior of the serum could be due to the adsorbed proteins rubbing against each other. According to the published results the proteins of the serum gets adsorbed on the different surfaces in different ways which is the reason for the different friction exhibited by the different materials in serum[126].

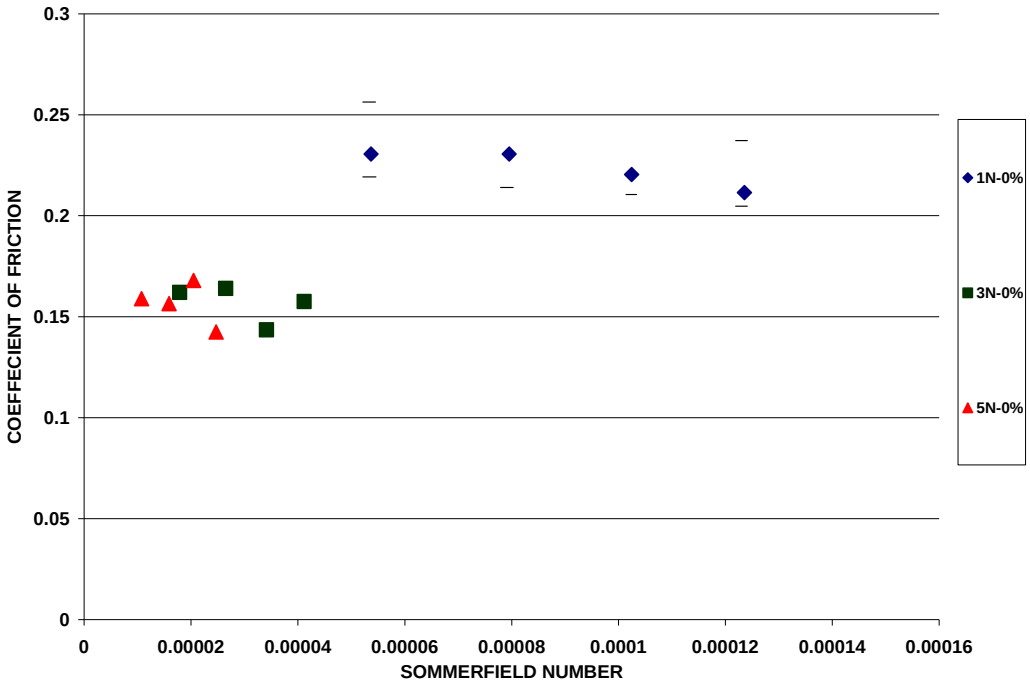

Figure 5.4. Stribeck plot 0% concentration.

Figure 5.5, i.e. with 25% concentration shows an upward trend for both of the cases which indicates full fluid film lubrication regime i.e. the load is carried by the lubricant entirely, In this regime the lubrication and the friction is controlled by the viscosity of the lubricant rather than the surface asperities. As seen from Figure 5.2, the viscosity is highest for the 25% concentration and hence high viscosity plays an important role for changing the lubrication mode to full fluid film lubrication regime for the higher load. For 50% concentration the lower load shows full fluid film lubrication regime whereas the higher loads shows mixed lubrication regime as seen in the figure 5.6. The lower viscosity observed at 50% concentration could be the reason for the higher loads showing mixed lubrication behavior.

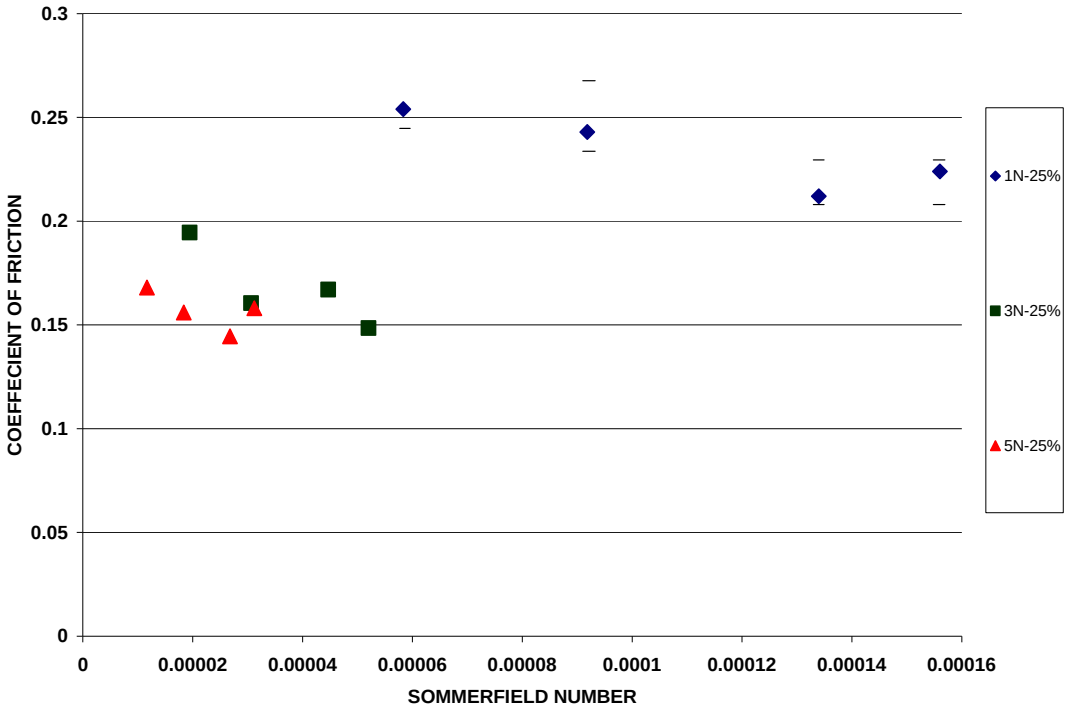

Figure 5.5. Stribeck plot for 25% concentration.

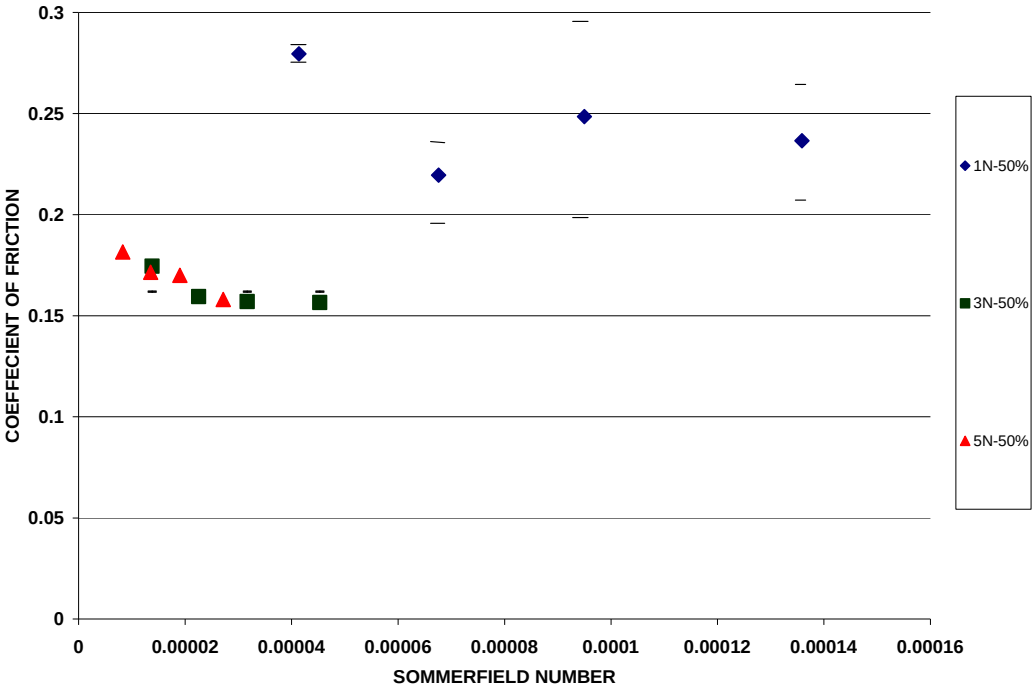

Figure 5.6. Stribeck plot for 50% concentration.

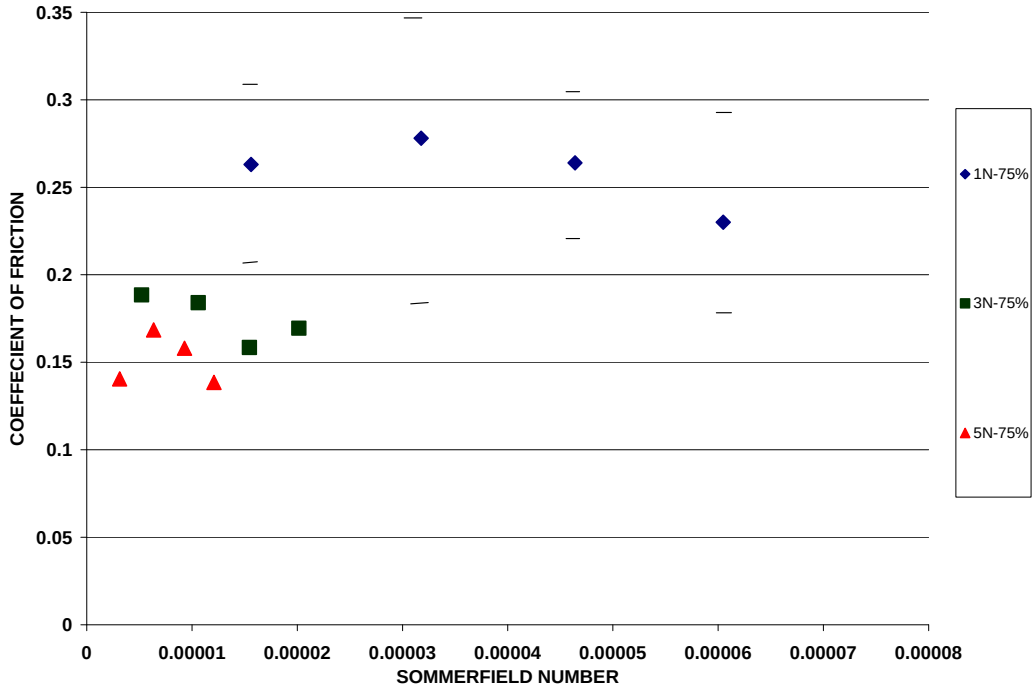

Figure 5.7. Stribeck plot for 75% concentration.

Figure 5.7 shows Stribeck plot for 75% concentration, both the cases show mixed lubrication behavior. For the higher load this is due to the low viscosity and high shear stress whereas for the lower load it is due to the protein-nanoparticle interaction.

The different behavior exhibited by the different concentration solutions at lower load is due to the interaction between the protein and the nanoparticles. Protein-nanoparticle interaction is also responsible for different viscosity and shear stress behavior. These interactions in the solution could be due to the following two forces:

1. Electrostatic attractive forces
2. Repulsive force

To understand the interaction better it is imperative to understand protein and the structure of the protein. Proteins are composed of amino acids. There are 20 different types of amino acids which get arranged in a specific way to form different types of proteins. These amino acids have an amino group on one side, a carboxyl group on the other, a third bond with hydrogen and fourth bond with variable side chain (R)[127]. Depending upon the reactive group, the 20 amino acids can be divided into three groups: first category contains apolar reactive group, the second category consists of uncharged polar R group and the third the charged R groups[128]. The charged group could be either positive or negative.

Since the protein has both positively and negatively charged amino acids, the proteins arrange the amino acids in such a way that there are positively charged regions and negative ones in the protein chain[129]. Figure 5.8 shows the structure of a serum albumin. The structure was created using the software PyMOL. The blue and the red

color represent the third category of the amino acid, i.e. charged amino acids or Lysine, Arginine, Aspartic acid and Glutamic acid

There may be electrostatic interactions between the amino acids present in the protein and the nanoparticles due to the difference of their charge[130]. Figures 5.9 and 5.10 show the chemical structure of Glutamic acid and Aspartic acid respectively. Both of these amino acids are negatively charged or acidic amino acids[131] and thus could bind electrostatically to the positively charged nanoparticles.

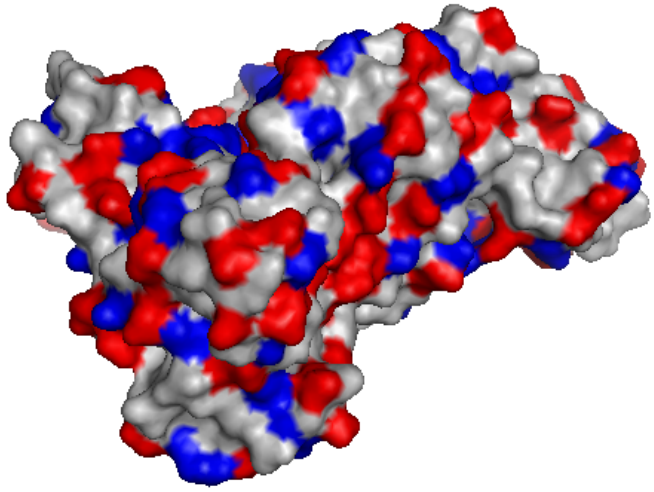

Figure 5.8. Structure of the albumin protein.

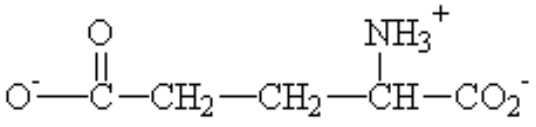

Figure 5.9. Chemical structure of the Glutamic acid.

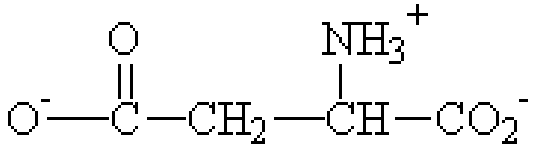

Figure 5.10. Chemical structure of the Aspartic acid.

As can be seen from the figures, the positive charge on the amine group and the negative charge on one of the carboxyl groups balance with each other. But the balance charge on the acid is still negative. These amino acids may interact with the positively charged nanoparticles. The electrostatic force is stronger than the Van der Walls bonding, thus the protein-nanoparticle bonding is very strong. This force leads to the proteins getting adsorbed around the nanoparticle surface in the form of a 'corona' because the nanoparticles have a very large surface-to-volume ratio and thus even small amount of particles will have a large surface area for the proteins to bind[132]. The affinity of the protein to the nanoparticle and their association is dynamic and changes over time. Figure 5.11 shows a pictorial representation of a corona of protein around the nanoparticle.

The other force is the repulsive force acting between the positively charged nanoparticles and the positive regions of the protein. Lysine and Arginine form the positively charged region of the protein and have a net positive charge[131].

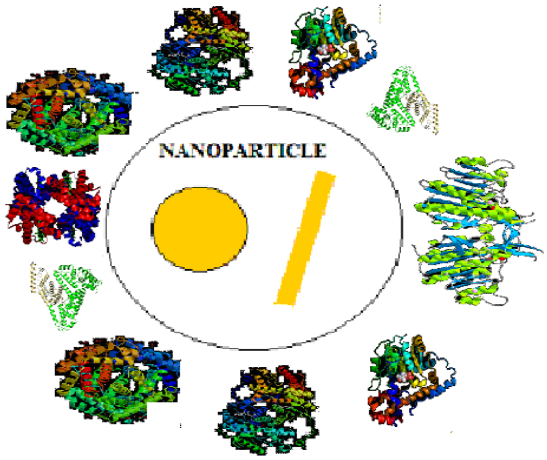

Figure 5.11. A pictorial representation of a protein corona around a nanoparticle.

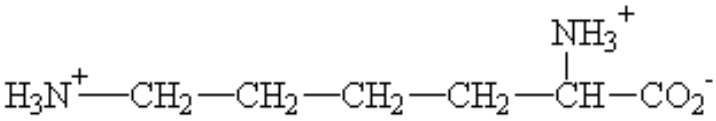

Figure 5.12. Chemical structure of Lysine.

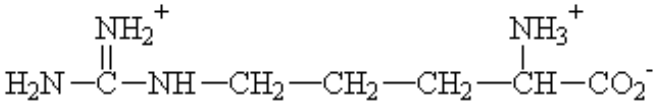

Figure 5.13. Chemical structure of Arginine.

As can be seen from the figures 5.12 and 5.13, there is a net positive charge on these amino acids and could have a repulsive interaction with the positively charged nanoparticles.

Figure 5.14 shows a pictorial representation of the possible interactions occurring between the protein and the nanoparticles at different concentrations. For 0%

concentration, there is only interaction between the serum molecules as seen in 5.14(a). For nanoparticles of 25%, 50% and 75% concentrations, with the addition of the nanoparticles to serum there is interaction between the nanoparticles and the protein. Now, there is protein-protein and protein-nanoparticle as seen in figures 5.14(b), 5.14(c) and 5.14(d). For the 25% and 50% concentration of nanoparticles, both the repulsive forces and the electrostatic forces exist and the electrostatic attraction dominates. Whereas for the 75% concentration, the large number of nanoparticles result in the domination of repulsive forces.

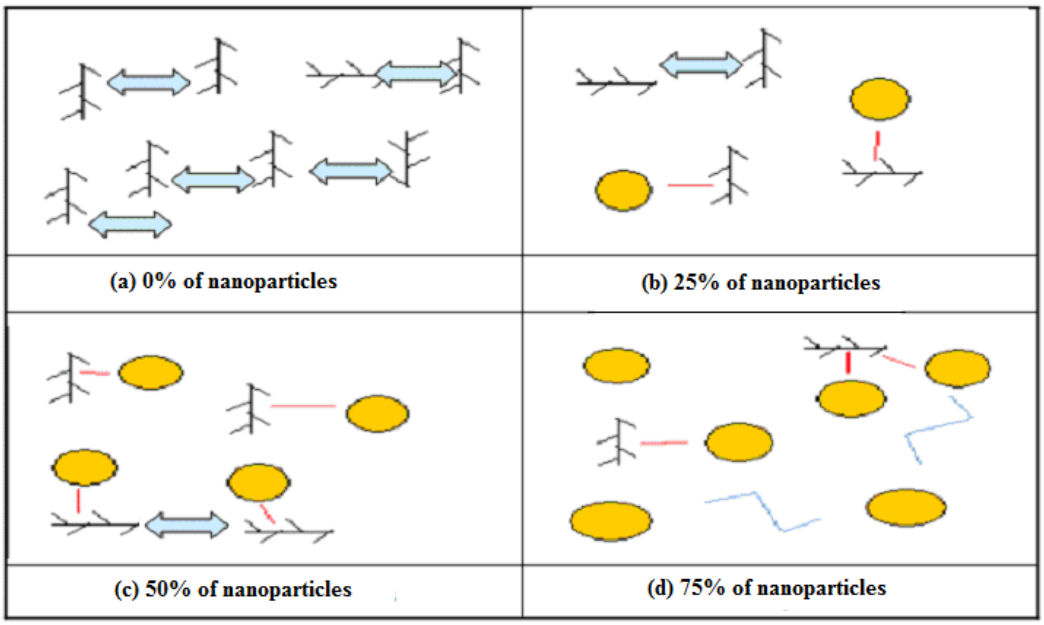

Figure 5.14. A schematic representation of all the four concentrations.

In order to validate the results obtained using the bovine serum, which had many proteins, enzymes and other metals, the same experiment was carried out using egg white. The egg white contains mainly the protein albumin. Figure 5.15 shows the

Stribeck plot obtained on mixing different concentrations of nanoparticles (25%, 50% and 75%) with the egg white at different speeds but at the load of 3N.

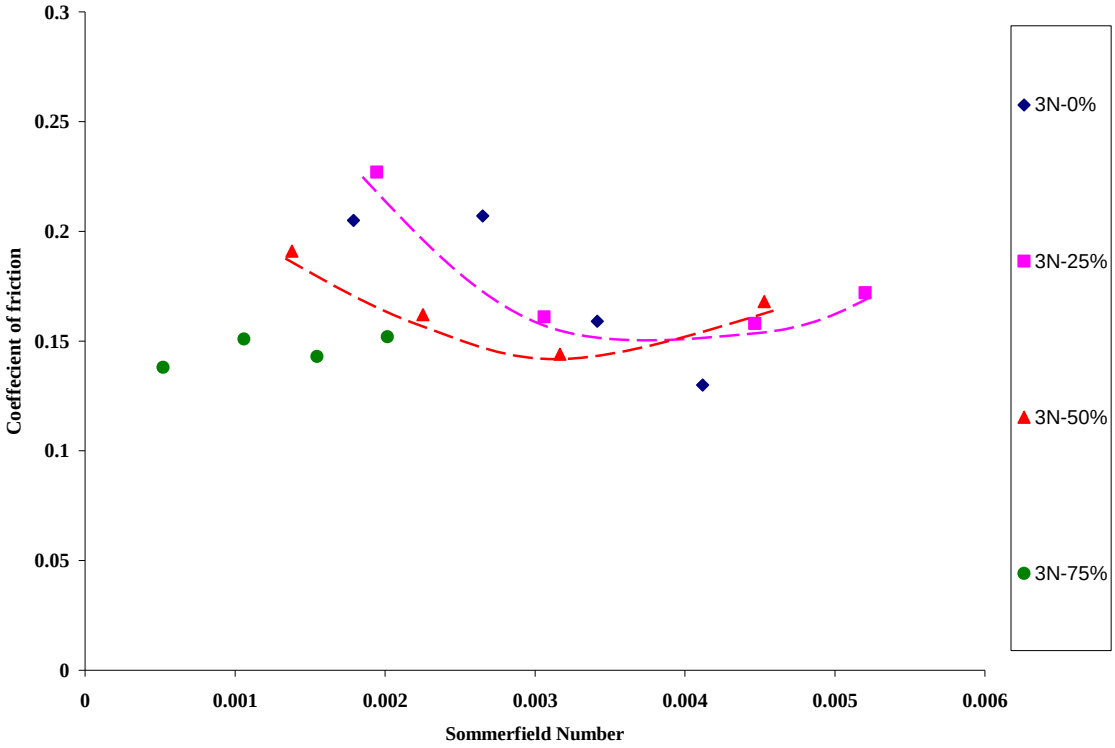

Figure 5.15. Stribeck plot for the egg at 3N load.

The results obtained here are similar to that obtained using the bovine calf serum and spherical nanoparticles. 0% and 75% show mixed lubrication regime whereas 25% and 50% show full fluid film lubrication regime. This validates the behavior predicted for the protein-nanoparticle interaction.

5.2.2 Rod-shaped nanoparticles

The same "Stribeck plot" was created for the rod-shaped nanoparticles to study their effect on the lubrication. The resulting Stribeck plot for all the concentrations is shown in the figure 5.16. All four concentrations do not show any trend i.e. they show boundary lubrication behavior for both high load and low load. They show high friction as compared to the spherical nanoparticles.

The high friction could be due to the difficulty in aligning these nanoparticles. In other words, the low coefficient of friction exhibited by the spherical nanoparticles as compared to the rod shaped nanoparticles and the change in the lubrication mode indicates that the spherical nanoparticles roll over each other. The schematic diagram of the rod and spherical nanoparticles are shown in figure 5.17.

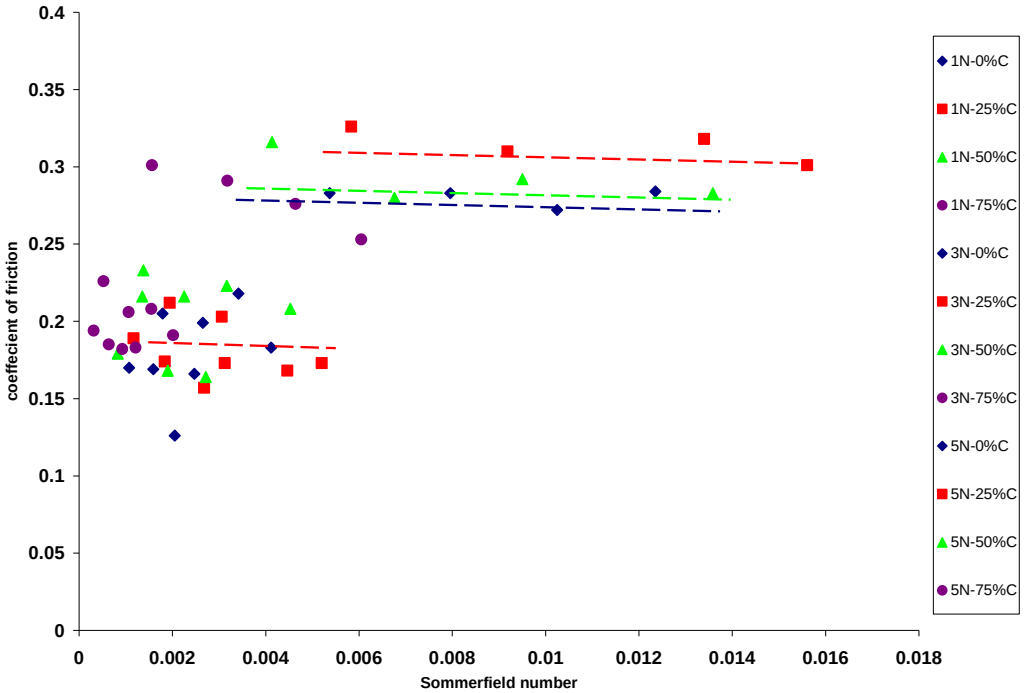

Figure 5.16. Stribeck plot for the rod-shaped nanoparticles.

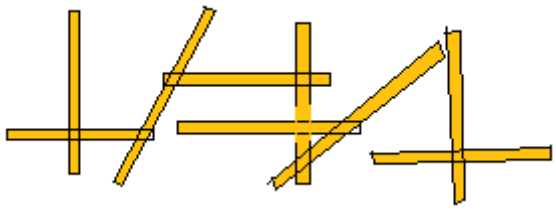

(a)

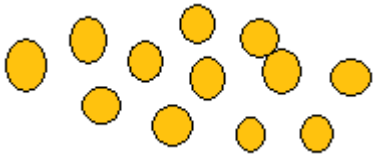

(b)

Figure 5.17. The arrangement of spherical and rod-shaped nanoparticles in the solution.

5.3 Surface Morphology

The surface morphology for the 25%, 50% and 75% concentration of nanoparticles were studied using a TEM. The before and the after tests images for the three concentrations were considered to determine the effect of nanoparticles. Figure 5.18(a), 5.19(a) and 5.20(a) were the before images. These images clearly showed the nanoparticles on the edge of the serum molecules; the grey area showing the serum molecules whereas the dark region showing the gold nanoparticles. Also it could be observed that with the increase in the concentration the amount of nanoparticles on the edge of the serum molecules had also increased. The nanoparticles tend to aggregate in the presence of salts[133]. As shown in the table 3.3, there are salts present in the serum, thus aggregating the nanoparticles which can be seen on the edge of the serum molecules. Also these chunks of aggregation have increased on going from 25%

concentration to 75% concentration. Figure 5.20(a) i.e. 75% concentration showed largest aggregation on the side due to more number of nanoparticles present in the solution as compared to the 50% and 25% concentration.

Figures 5.18(b), 5.19(b) and 5.20(b) showed the changes in the surface morphology after the tribometer tests, it could be seen that the nanoparticles were no longer only at the edges but they were seen covering the serum molecules. This was visible from the change of color from light gray to dark gray. This could be explained using the Newton's classical model of fluid friction which states that the fluid film between the two mating surfaces can be separated into many thin layers. Thus when the tests were run on the tribometer, these layers swept past each other bringing nanoparticles into contact with the proteins on the other layers. Due to the electrostatic interaction between the positively charged nanoparticles and the negative regions of the protein, they bind to each other. This is visible from the change in the images of before and after the tribology tests for all the three concentration of nanoparticles.

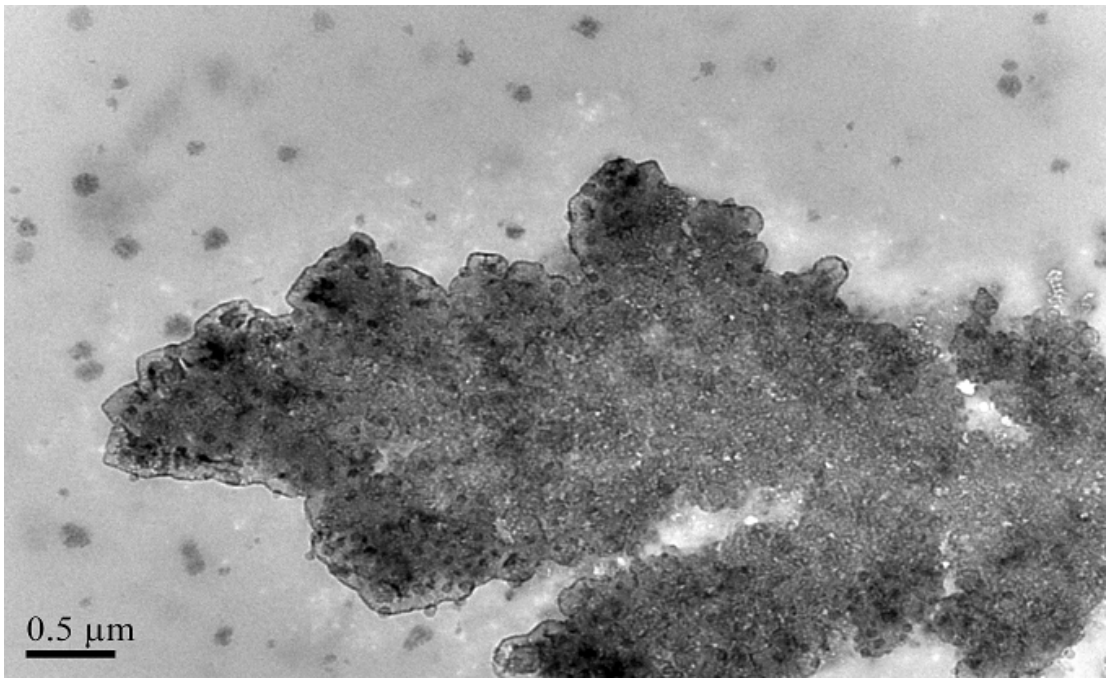

(a)

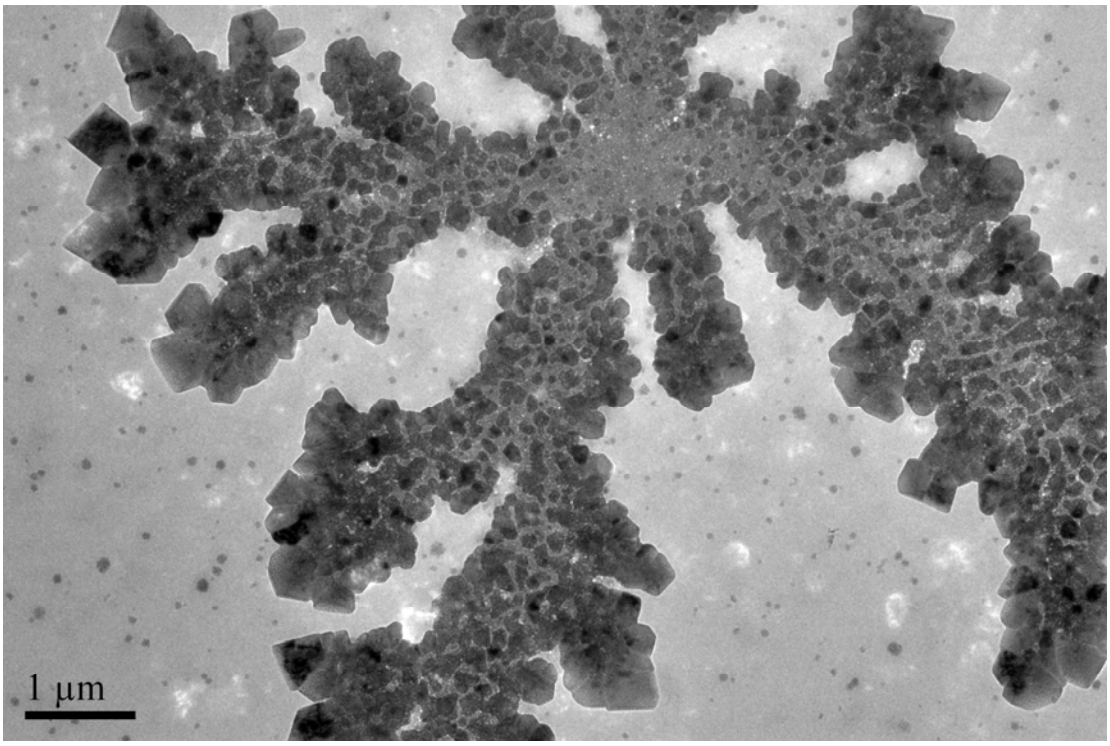

(b)

Figure 5.16. The before and after TEM images of 25% concentration.

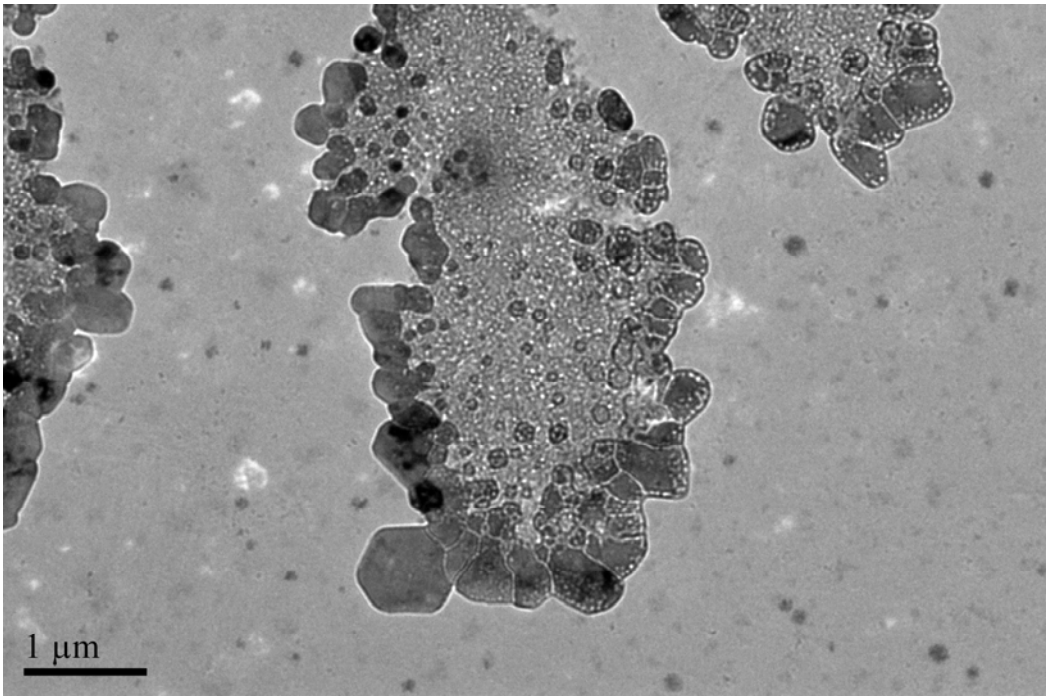

(a)

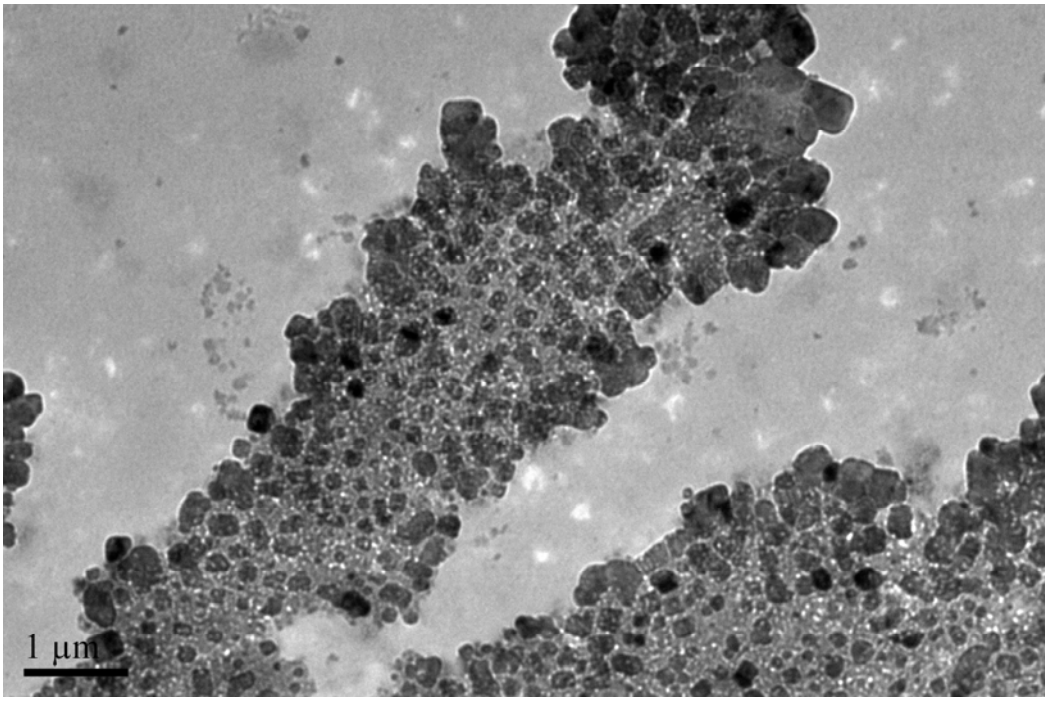

(b)

Figure 5.17. The before and after TEM images of 50% concentration.

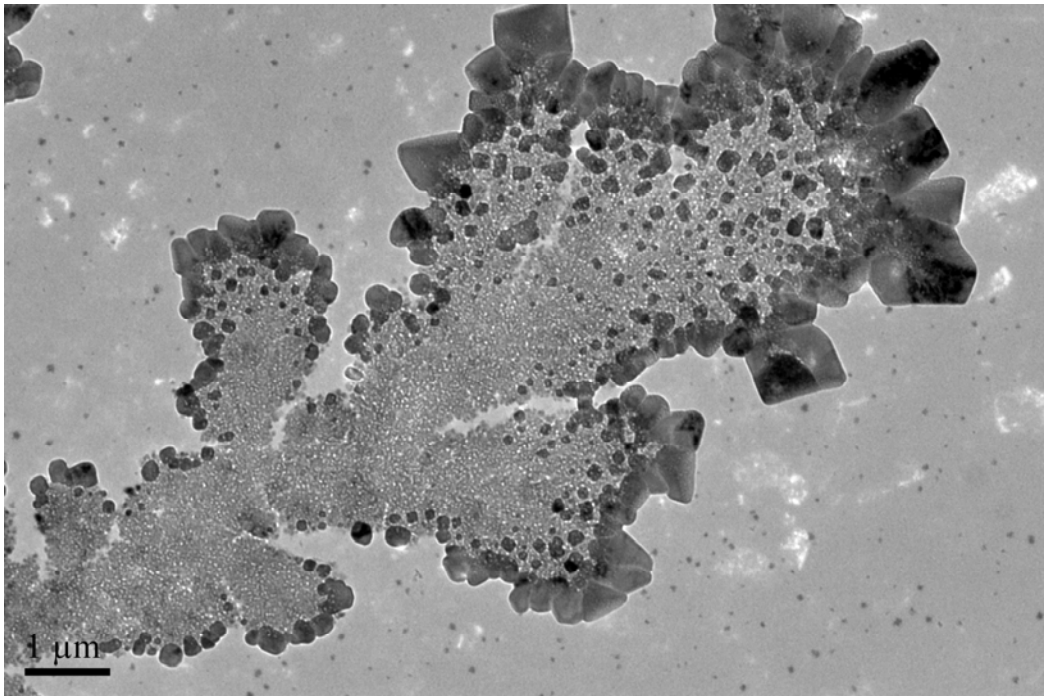

(a)

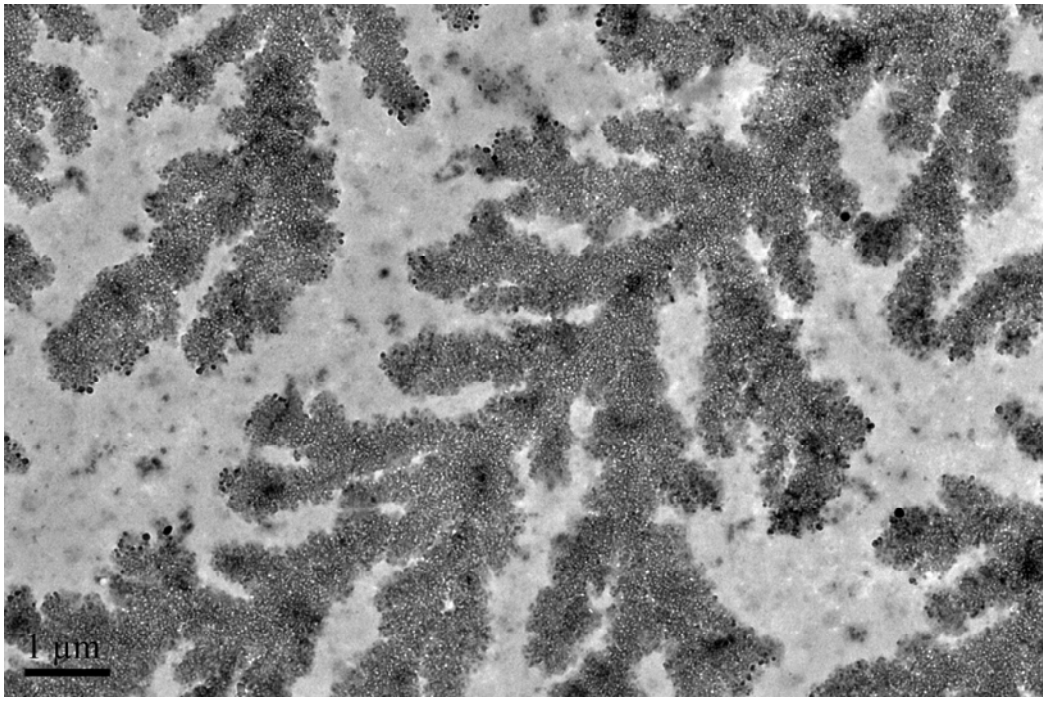

(b)

Figure 5.18. The before and after TEM images of 75% concentration.

5.4 Remarks

Different concentrations of spherical and rod-shaped nanoparticles were mixed with bovine calf serum and tested on a pin-on-disk tribometer to generate “Stribeck” curves. It was found that the spherical nanoparticles exhibited lower friction as compared to the rod ones. In addition, two different frictional behaviors were observed, one for the lower load and one for the higher load. Evidence indicates that here are two competing mechanisms dominating the lubrication behavior of fluids, fluid flow and the fluid flow and protein-nanoparticle interactions.

The solution with 25% nanoparticles showed a full fluid film lubrication regime for both higher and lower load due to high viscosity and electrostatic interaction between the positively charged nanoparticles and the positive regions of the protein.

The 50% solution showed mixed lubrication at higher load which could be due to lower viscosity while the solution showed full fluid film lubrication regime for the lower load due to the electrostatic interactions between the nanoparticles and the protein.

The 75% showed mixed lubrication for both the cases because of lower viscosity, higher shear stress and repulsive force dominating the nanoparticle and the protein interactions.

The TEM image of before and after the tribology tests further proved that there was interaction between the protein and the nanoparticles. Also, the interactions between the protein and the nanoparticles have lead to the different lubrication behavior.

6. CONCLUSIONS

This thesis research studied tribological properties of ceramic coatings and nanoparticle-modified biofluids potentially to be used for artificial joints. Two areas of investigation were conducted. Firstly, we studied the effects of the microstructures of the coatings on friction and wear. Secondly the synthetic biofluid was modified using nanoparticles and their interfacial interactions were investigated. The results obtained from both of these experiments led to the following conclusions and possible future work.

6.1. Conclusions

6.1.1 Tribological study of the MAO coatings

1. The frictional behavior depends on the relative hardness of ball-on-disk materials. It was found that an increase in the α-Al_2O_3 and the γ-Al_2O_3 phase with an increase in the current intensity was found to reduce the friction. Therefore, the 0.150 A/cm^2 showed the lowest mean friction among all the three MAO coatings.
2. Since the debris filled up the opened discharge channels, there was only redistribution of the mass and thus the wear on the MAO coating was not calculable. Using the SEM images, the wear mechanisms were found to be abrasive with micro fracture.

3. Due to the low co-efficient of friction and low wear, the MAO coating was found to be highly wear resistant in the biofluid environment and could be used for biological implants.

6.1.2 Lubrication study of the gold nanoparticles

1. The 25% and 50% concentrations of nanoparticles show full fluid film lubrication regime which can be seen from the Stribeck plot for the calf serum as well as the egg.
2. The interaction between the protein and the nanoparticles has lead the different concentration solution to show different lubrication behavior
3. The interactions between the protein and the nanoparticle involve two mechanisms: electrostatic interactions between the positively charged gold nanoparticles and the negative regions of the proteins; and repulsive force between the positively charged regions of the protein and nanoparticle as well as between two nanoparticles. A model was developed to highlight such interactions.

6.2 Recommendations

1. Characterization of protein-nanoparticle interactions.
2. Develop a technique to be able to test the amount of electrostatic force and the repulsive force.
3. Optimize the biofluids useful for artificial joints.

REFERENCES

[1] J. H. Peter, Tribology: How a word was coined 40 years ago, Tribology & Lubrication Technology (2006).

[2] J. E. Pope, *Rules of Thumb for Mechanical Engineering* (Gulf Professional Publishing, Houston, 1996) p. 227.

[3] S.K. Basu, S.N. Sengupta and B.B. Ahuja, *Fundamentals of Tribology* (Prentice-Hall of India Pvt. Ltd., New Delhi, 2005).

[4] L. B. Sibley, M. Zlotnick and T. M. Levinson, Battelle Memorial Inst. (Pacific Northwest Labs, Richland, WA, 1985)

[5] D. Dowson, *History of Tribology* (Longman, London, 1979).

[6] A. Z. Szeri, *Fluid Film Lubrication: Theory & Design* (Cambridge University Press, Cambridge, 1998).

[7] B. Bhushan, *Introduction to Tribology* (John Willey and Sons, New York, 2002).

[8] W. H. McNeill, *The rise of the West: A History of the Human Community* (University of Chicago Press, New York, 1963).

[9] C. St. C. Davidson, Technology and Culture 2 (1961) 11-16.

[10] E. Macurdy, *The Notebooks of Leonardo da Vinci* (Reynal & Hitchcock, New York, 1938).

[11] A. E. H. Love, *Treatise on the Mathematical Theory of Elasticity* (Dover Publications, New York, 1944).

[12] D. L. Hire, Histoire de l' Academie Royale des Sciences (1699) 104.

[13] C. A. Coulomb, Academie Royale des Sciences (1785) 612-638.

[14] O. Reynolds, Phil. Trans. Roy. Soc. A177 (1886) 157-234.

[15] N. P. Petrov, Inzh. Zfc. St-Peterb. 1 (1883) 71-140.

[16] N. P. Petrov, Inzh. Zfc. St-Peterb. 2 (1883), 227–279.

[17] N. P. Petrov, Inzh. Zfc. St-Peterb. 3 (1883) 377–463.

[18] N. P. Petrov, Inzh. Zfc. St-Peterb. 4 (1883) 535–564.

[19] B. Tower, Proc. Inst. Mech. Engrs. (1883) 632-659.

[20] B. Tower, Proc. Inst. Mech. Engrs. (1885) 58-70.

[21] R. Temam, *Navier-Stokes Equation: Theory and Numerical Analysis* (AMS Bookstore, New York, 2001)

[22] F. Archibald, History of Lubrication: Anthony G. M. Mitchell, Lubrication Engineering (2000).

[23] S. R. Majumdar, *Oil Hydraulic systems: Principle and Maintenance* (McGraw hill Professional, New York, 2005).

[24] D. Dawson, *History of Tribology (2nd edition)* (Professional Engineering Publishing Ltd., London, 1998).

[25] A. A. Seireg, *Friction and Lubrication in Mechanical Design* (Marcel Dekker Inc., New York, 1998).

[26] T. Mang and W. Dresel, *Lubricants and Lubrication*, (Wiley-vch, Weinheim, 2007).

[27] B. N. J. Persson and E. Tosatti, *Physics of Sliding Friction: Proceedings of the NATO Advanced Research* (Springer, The Netherlands, 1996).

[28] C. L. Rao, J. Lakshminarasimhan, R. Sethuraman and S. M. Sivakumar, *Engineering Mechanics: Statics and Dynamics* (Prentice-Hall of India Pvt. Ltd., New Delhi, 2003) p. 123.

[29] C. E. Fuller, W. A. Johnston, *Applied Mechanics* (John Willey & Sons, New York, 1913).

[30] B. Bhushan, *Principles and Applications of Tribology* (John Willey & Sons, New York, 1999)

[31] M. LaBerge, *Handbook of Biomaterial Properties* (Chapman & Hall, London, 1998).

[32] G. R. Miller, L. M. Keer and H. S. Cheng, Proc. Roy. Soc. A397 (1985) 197-209.

[33] F. R. Young, *Cavitation* (Imperial College Press, London, 1999).

[34] R.B. Waterhouse, ASM Handbook, Friction, Lubrication and Wear Technology 18 (1992) 242–256.

[35] R. Stribeck, *Zeit* Ver, Duet. Ing. 46 (1902) 1341-1348.

[36] M. D. Hersey, J. Wash. Acad. Sci. 4 (1914) 542-552.

[37] F. P. Bowden and D. Tabor, *The Friction and Lubrication of Solids* (Clarendon Press, Oxford, 2001)

[38] A. Harnoy, *Bearing Design in Machinery: Engineering Tribology and Lubrication* (CRC Press, Boca Raton, 2003*).*

[39] D. Dowson and Z-M Jin, Proc. Instn. Mech. Engrs. Part H: J. Engineering in Medicine 220 (2006) 107-118.

[40] S. C. Scholes, A. Unsworth, R. M. Hall and R. Scott, Wear 241 (2000) 209-213.

[41] S. L. Smith, D. Dawson and A. A. J. Goldsmith, Proc. Instn Mech Engrs. Part J: J. Engineering in Medicine 215 (2001) 483-493.

[42] S. C. Scholes and A. Unsworth, Proc. Instn. Mech. Engrs. Part H: J. Engineering in Medicine 220 (2006) 687-693.

[43] S. C. Scholes, A. Unsworth, Proc. Instn. Mech. Engrs. Part H: J. Engineering in Medicine 214 (2000) 49-57.

[44] I. M. Hutchings, *Friction, Lubrication, and Wear of Artificial Joint* (Professional Engineering Publishing, London, 2003) p. 1-6.

[45] H. Reul, C. Schmitz, EM Pfaff, C. Hohlstein, PA Schmidt, G. Rau and P. Arru, J. Heart Valve Dis. 11 (2002) 409-418.

[46] F. J. Holly and T. F. Holly, *Advances in Ocular Tribology. In: Lacrimal Gland, Tear Film, and Dry Eye Syndromes* (Plenum Press, New York, 1994) p. 275-283.

[47] W. Hou, W. Bingjie, J. Z. Yongzhong, Z. Qi, Z. Li, H. Y. Double, L. Hung, W. Jingying, Biological Comm. 12 (2005).

[48] L. S. Pinchuk, V. I. Nikolaev, E. A. Tsvetkova, *Tribology and Biophysics of Artificial Joints* (Elsevier, London, 2006).

[49] D. Dowson and A. Neville, Proc. Instn. Mech. Engrs. Part J: J. of Engineering Tribology 220 (2006) 109-123.

[50] J. H. Dumbleton, *Tribology of Natural and Artificial Joints* (Elsevier Scientific Pub. Co., Amstradam, 1981).

[51] K. Premkumar, *The Massage Connection: Anatomy & Physiology* (Lippincott Williams & Wilkins, Baltimore, 2003).

[52] D. Layman, *Anatomy Demystified* (McGraw-Hill Professional, New York, 2004)

[53] D. A. B. Archer, C. W. Archer, D. B Archer, B. Caterson, M. Benjamin and J. R. Ralphs, *Biology of the Synovial Joint* (Informa Health care, Amstradam, 1999).

[54] R. M. Enoka, *Neuromechanics of Human Movement* (Human Kinetics, Champaign, Illinois, 2002).

[55] B. J. Cole and M. M. Malek, *Articular Cartilage Lesions: A Practical Guide to Assessment and Treatment* (Springer, New York, 2004) p. 3.

[56] W. C. Whiting and S. Rugg, *Dynatomy: Dynamic Human Anatomy* (Human Kinetics, Champaign, Illinois, 2005) p. 41.

[57] M. Kobayashi and M. Oka, Bio-Medical Mat. Engg. 13 (2003) 429-437.

[58] H. J. Mankin, J. Bone Jt. Surg. 64-A (1982) 460-466.

[59] K. Lorig. J. F. Fries and M. R. Gecht-Silver, *The Arthritis Helpbook* (Da Capo Press, Cambridge, 2005).

[60] S. C. Lewis, *Providing for the Older Adult: A Gerontological Handbook* (Slack Inc., Thorofare, NJ, 1983)

[61] W. Zhang, A. Jones and M. Doherty, Annals of the Rheumatic Diseases 63 (2004) 901-907.

[62] T. F. Dougherty and G. L. Schneebeli, Annals of the New York Academy of Sciences 61 (1955) 328–348.

[63] R. M. Meneghini, N. J. Hallab and J. J. Jacobs, Instr Course Lect. 54 (2005) 481-93.

[64] P. Campbell, F. W. Shen and H. McKellop, Clin Orthop Relat Res. 418 (2004) 98-111.

[65] D. G. Poitout, *Biomechanics and Biomaterials in Orthopedics* (Springer, New York, 2004).

[66] Joint Replacement Surgery, Weiss Memorial Hospital, Retrieved from www.weisshospital.com, date 20th April' 08.

[67] M. A. McGee, D. W. Howie, S. D. Neale, D. R. Haynes and M. J. Pearcy, Proc. Instn Mech. Engrs. Part H: J. Engineering in Medicine 211 (1997) 65-72

[68] A. S. Shanbhag, J. J. Jacobs, T. T. Grant, J. L. Gilbert, J. L. Black and J. O. Galante, J. Bone Jt. Surgery 76-B (1994) 60-67.

[69] R. M. Hall, A. Unsworth, P. Siney and B. M. Wroblewski, Proc. Instn. Mech. Engrs. Part H: J. Engineering in Medicine 210 (1996) 197-207.

[70] A. P. D. Elfick, R. M.Hall, I. M.Pinder and A. Unsworth, J. Arthroplasty 13 (1998) 291-295.

[71] Data on file at Biomet Manufacturing Corp. Bench Test Results Not Necessarily Indicative of Clinical Performance, Retrieved from www.biomet.com, date 1st April' 08.

[72] E. W. Soh, G. W. Blunn, G. W. Wait and P. S. Walker, Transactions of the 42nd Annual Meetings of the Orthopaedic Research Society (1996) 462.

[73] P. F. Doorn , P. A. Campbell , J. Worrall , P. D. Benya , H. A. McKellop and H. C. Amstutz, J. Biomed. Mat. Res. A42 (1998) 103-111.

[74] V. G. Langkamer, C. P. Case, P. Heap, A. Taylor, C. Collins, M. Pearse and L. Solomon, J. Bone Jt. Surgery 74-B (1992) 831-839.

[75] C. Lhotka , T. Szekeres , I. Steffan , K. Zhuber , K. Zweymüller, J. Orthop. Res. 21(2006) 189-195.

[76] A J Stewart, B M Southcott and E Raweily, J. Roy. Soc. Med. 96 (2003) 404–406.

[77] C. P. Case, V. G. Langkamer, C. James, M. R. Palmer, A. J. Kemp, P. F. Heap and L. Solomon, J. Bone Jt. Surgery 76-B (1994) 701-712.

[78] J. A. D'Antonio and M. Dietrich, *Bioceramics and Alternative Bearings in Joint Arthroplasty: 10th Biolox* (Springer, Germany, 2006) p.21.

[79] L. Savarino, M. Greco, E. Cenni, L. Cavasinni, R. Rotini, N. Baldini, and A. Giunti, J. Bone Jt. Surg. 88-B (2006) 472-476.

[80] F. J. Archard, J. Appl. Phys. 24 (1953) 981-988.

[81] N. D. L. Burger, P. L. Vaalb and J. P. Meyer, Engineering Failure Analysis 14 (2007) 1329-1345.

[82] S. Challa, S. R. Kumar, *Nanomaterials for Biosensors* (Willey-VCH, Weinheim, 2007).

[83] L. Kolodziejczyk, D. Martinez-Martinez, T. C. Rohas, A. Fernandez and J. C. Sanchez-Lopez, J. Nanoparticle Res. 9 (2007) 639-645.

[84] J. Zhou, J. Yang, Z. Zhang, W. Liu and Q. Xue, Mats. Res. Bulletin 34 (1999) 1361-1367.

[85] L. Sun, J. Zhou, Z. Zhang and H. Dang, Wear 256 (2004) 176-181.

[86] J. Zhou, Z. Wu, Z. Zhang, W. Liu and Q. Xue, Tribol. Lett. 8 (2000) 213-218.
[87] Q. Xue, J. Zhang and Z. Zhang, Wear 209 (1997) 8.

[88] K. S. Morley, P. B. Webb, N. V. Tokareva, A. P. Krasnov, V. K. Popov, J. Zhang, C. J. Roberts and S. M. Howdle, European Polymer Journal 43 (2007) 307-314.

[89] J. J. Jacobs, A. Shanbhag, T. T. Giant, J Black and J. O. Galante, J. Am. Acad. Orthop. Surg. 2 (1994) 212-220.

[90] CDC. Prevalence of Disabilities and Associated Health Conditions – U.S; 1991-1992, *MMWR* 1994: 43:730-1, 737-9.

[91] A. L. Yerokhin, X. Nie, A. Leyland, A. Matthews and S. J. Dowey, Surf. Coat. Technol. 130 (2000) 195-206.

[92] M. D. Klapkiv, Mater. Sci. 31 (1995) 494-499.

[93] X. Nie, A. Leyland, H. W. Song, A. L. Yerokhin, S. J. Dowey and A. Mathews, Surf. Coat. Technol. 116-119 (1999) 1055-1060.

[94] W. Sneader, *Drug Delivery: A History* (John Willey & Sons, London, 2005) p.60.

[95] M. Faraday, *Phil. Trans. Roy. Soc.* 14 (1857) 145.

[96] S. Kundu, S.K. Ghosh, M. Mandal and T. Pal, New J. Chem. 26 (2002) 1081-1084.

[97] S. Kundu, S.K. Ghosh, M. Mandal and T. Pal, New J. Chem. 27 (2003) 656-662.

[98] N. R. Jana and T. Pal, Langmuir 15 (1999) 3458-3463.

[99] N. R. Jana, T. K. Sau and T. Pal, J. Phys. Chem. B 103 (1999) 115-121.

[100] S. Link and M. A. El-Sayed, J. Phys. Chem. B 103 (1999) 4212-4217.

[101] P. V. Kamat, Chem. Rev. 93 (1993) 267-300.

[102] L. R. Hirsch, R. J. Stafford, J. A. Bankson, S. R. Sershen, B. Rivera, R. E. Price, J. D. Hazle, N. J. Halas and J. L. West, Proc. Natl. Acad. Sci. 100 (2003) 13549-13554

[103] N. P. Gaponik, D. V. Talapin and A. L. Rogach, J. Mater. Chem. 10 (2000) 2163-2166.

[104] M. B. Mohamed, K. Z. Ismail, S. Link and M. A. El-Sayed, J. Phys. Chem. B 102 (1998) 9370-9374.

[105] A. Pal, Talanta 46 (1998) 583-587.

[106] M. Brust, M. Walker, D. Bethell, D. J. Schiffrin and R. Whyman, Chem. Comm. (1994) 801-802.

[107] K. Esumi, A. Suzuki, A. Yamahira and K. Torigoe, Langmuir 16 (2000) 2604-2608.

[108] M. K. Corbierre, N. S. Cameron and B. R. Lennox, Langmuir 20 (2004) 2867-2871.

[109] C. S. Love, V. Chechik, D. K. Smith and C. Brennan, J. Mater. Chem. 14 (2004) 919-926.

[110] Assay of Bovine Calf Serum, (Hyclone Inc., 84321, Utah, 2007).

[111] C. Hatchett, Phil. Trans. Roy. Soc. 93 (1803) 43-194.

[112] TR 200 Portable Surface Profilometer, (Micro Photonics Inc., 18106, Pennsylvania, 2006).

[113] H. Stintzing, Verfahren und Einrichtung zum automatischen Nachweiss, Messung und Zählung von Einzellteilchen beliebiger Art, Form und Grösse. German patent No 485155 (1929).

[114] M. Knoll, Z. Tech. Phys. 16 (1935) 467-47.

[115] D. McMullan, "Scanning Electron Microscopy 1928 - 1965" Presentation, 51st Annual Meeting of the Microscopy Society of America, Cincinnati, August 1993.

[116] M. Knoll and E. Ruska, Ann Physik 12 (1932) 607-661.

[117] J. J. Bozzola and L. D. Russell, *Electron Microscopy: Principles and Techniques for Biologists* (Jones & Bartlett Publishers, Massachusetts, 1999) p. 148-201.

[118] AR-G2 Rheometer, Retrieved from Product Manual-TA Instruments (2008).

[119] Vendittoli, J. Girard, M. Lavigne, P. Lavoie and N. Duval, Acta Orthopaedica Belgica 73 (2007) 468-477.

[120] S. G. Xin, L. X. Song, R. G. Zhao and X. F. Hu, Mater. Chem. Phys. 97 (2006) 132-136.

[121] G. Sundararajan and L. Krishna, Surf. Coat. Tech. 167 (2003) 269-277.

[122] S. H. Teoh, International Journal of Fatigue 22 (2000) 825-837.

[123] R. Rosencranz, and Steven A. Bogen, Am J Clin Pathol 125 (2006) S78-*S86*

[124] S. B. Devarakonda, J. Han, C. H. Ahn and R. K. Banerjee, Microfluidics and Nanofluidics 3 (2007) 391-401.

[125] S. C. Scholes, A. Unsworth, Proc. IMech Engg Part H: J. Engineering in Medicine, 220 (2006) 687-693.

[126] I. M. Hutchings, *Friction, Lubrication and Wear of Artificial Joints: Tribology Meets Medical* (John-Wiley & Sons, New York, 2003) p.58-74.

[127] G. L. Zubay, *Biochemistry* (Macmillan Pub. Co., New York, 1998).

[128] C. Branden, J. Tooze, *Introduction to Protein Structure* (Garland, New York, 1991).

[129] G. Buckton, *Interfacial Phenomena in Drug Delivery and Targeting* (CRC Press, Boca Raton, Florida, 1995) p. 240.

[130] O. Horovitz, G. Tomoaia, A. Mocanu, T. Yupsanis and M. Tomoaia-Cotisel, Gold Bulletin 40 (2007) 213-218.

[131] I. M. Rosenberg, *Protein Analysis and Purification: Benchtop Techniques* (Springer, Verlag, 69121, Germany, 2004) p. 11.

[132] J. Klein, Proc. Natl Acad Sci USA 104 (2007) 2029-2030.

[133] K. Cho, Y. Lee, C. Lee,K. Lee, Y. Kim, H. Choi, P. Ryu, S. Yeong Lee and S-W Joo, J. Phys. Chem. 112 (2008) 8629–8633.

[134] V. Vanchikov, Russian Engg. Res. 27 (2007) 35-39.

VITA

Juhi Bhaskar Baxi received her Bachelor of Engineering degree in mechanical engineering from L.D. College of Engineering, Gujarat University at Ahmedabad, India in 2006. She entered the mechanical engineering program at Texas A&M University in the spring of 2007 and received her Master of Science degree in the summer of 2008. Her research interests are in the tribological characterization of low friction and low wear coatings and in the development of new lubricants.

Ms Baxi may be reached at Technip Inc., 11700 Katy Freeway, Houston, Texas 77079. Her email is juhi.baxi@gmail.com. Her contact information may also be found from her advisor Dr Hong Liang of the Mechanical Engineering Department at Texas A&M University, College Station TX 77843-3123.